Modeling the 26 December 2004 Indian Ocean tsunami: Case study of impact in Thailand

M. Ioualalen,[1] J. Asavanant,[2] N. Kaewbanjak,[2] S. T. Grilli,[3] J. T. Kirby,[4] and P. Watts[5]

[1] The devastating 26 December 2004 Indian Ocean tsunami stressed the need for assessing tsunami hazard in vulnerable coastal areas. Numerical modeling is but one important tool for understanding past tsunami events and simulating future ones. Here we present a robust simulation of the event, which explains the large runups and destruction observed in coastal Thailand and identifies areas vulnerable to future tsunamis, or safer for reconstruction. To do so, we use an accurate tsunami source, which was iteratively calibrated in earlier work to explain the large-scale tsunami features, and apply it over a computational domain with a finer grid and more accurate coastal bathymetry in Thailand. Computations are performed with a well-validated numerical model based on fully nonlinear and dispersive Boussinesq equations (FUNWAVE) that adequately models the physics of tsunami propagation and runup, including dissipation caused by bottom friction and wave breaking. Simulated runups in Thailand reproduce field observations with a surprising degree of accuracy, as well as their high degree of along-coast variation: a 92% correlation is found between (58) runup observations and computations, while the model explains 85% of the observed variance; overall, the RMS error is approximately 1 m or 17% of the mean observed runup value (skill of the simulation). Because we did not use runup observations to calibrate our coseismic tsunami source, these results are robust, and thus provide a uniquely accurate synoptic prediction of tsunami impact along the Andaman coast of Thailand, including those areas where no observations were made.

Citation: Ioualalen, M., J. Asavanant, N. Kaewbanjak, S. T. Grilli, J. T. Kirby, and P. Watts (2007), Modeling the 26 December 2004 Indian Ocean tsunami: Case study of impact in Thailand, *J. Geophys. Res.*, *112*, C07024, doi:10.1029/2006JC003850.

1. Introduction

[2] The megathrust earthquake that struck near Indonesia on 26 December 2004 at 0h58′53″ UTC (+7h for Thailand local time) was likely the 3rd largest earthquake ever recorded [*Stein and Okal*, 2005]. From its epicenter, located 80 km west of the coast of northern Sumatra (at approximately 95°51′W, 3°25′N), the earthquake proceeded approximately northward, rupturing 1200–1300 km of the Andaman-Sunda trench in about 8–10 min [*Ammon et al.*, 2005; *Lay et al.*, 2005] (Figure 1). Liberating enormous energy, corresponding to a $M_w \simeq 9.3$ moment magnitude, the earthquake triggered a tsunami that was one of the most devastating natural disasters ever witnessed in modern history, causing more than 292,000 fatalities in 12 countries bordering the Indian Ocean basin (T. Kawata et al., The December 26, 2004 earthquake tsunami disaster of Indian Ocean. Research Group on The December 26, 2004 Earthquake Tsunami Disaster of Indian Ocean, 2006, http://www.drs.dpri.kyoto-u.ac.jp/sumatra/index-e.html#casualty) (hereinafter referred to as Kawata et al., online report, 2006). The largest tsunami runups, over 30 m, occurred south of Banda Aceh, Sumatra, whose shore is closest to the epicenter, only about 10 minutes away in terms of tsunami propagation time (Figure 1). This area suffered the majority of fatalities (almost 230,000 dead or missing) and the most intense and widespread destruction during the 12/26/04 event (T. Kawata et al., Comprehensive analysis of the damage and its impact on coastal zones by the 2004 Indian Ocean tsunami disaster, 2005, Disaster Prevention Research Institute, http://www.tsunami.civil.tohoku.ac.jp/sumatra2004/report.htm, 2005) (hereinafter referred to as Kawata et al., online report, 2005). The next most heavily impacted area was the coast of Thailand, although it is located on the other side of Sumatra, not in direct line of the epicenter. It took the tsunami 1h45′ to 2h to reach this location [*Tsuji et al.*, 2006]. Thousands of fatalities occurred in Thailand even though, on this east side of the fault, the first tsunami wave to arrive was a large depression wave that caused a significant withdrawal of the ocean at many locations, a crucial sign of tsunami arrival that often was not correctly read.

[3] All of the six Thai provinces that border the Andaman coast (Ranong, Phang Nga (Khao Lak area), Phuket, Krabi,

[1]Geosciences Azur, IRD-CNRS-UPMC-UNSA, Villefranche-sur-Mer, France.

[2]Department of Mathematics, Chulalongkorn University, Bangkok, Thailand.

[3]Department of Ocean Engineering, University of Rhode Island, Narragansett, Rhode Island, USA.

[4]Center for Applied Coastal Research, University of Delaware, Newark, Delaware, USA.

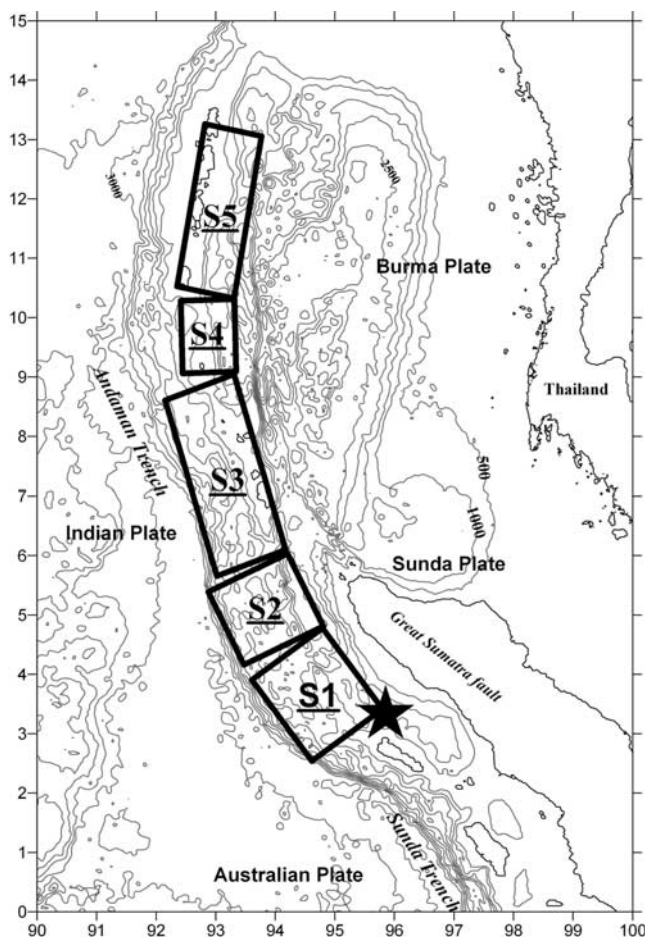[5]Applied Fluids Engineering, Inc., Long Beach, California, USA.

Figure 1. ETOPO2 bathymetry around the 26 December 2004 earthquake location (star) contoured at 500-m intervals. Rectangles S1–S5 represent the *Okada* [1985] dislocation model fault segments (Table 1).

Trang, and Satun; Figures 2–5) have exposed coastlines that were severely damaged by the tsunami. Among these, the province of Phang Nga suffered the most fatalities, accounting for 71% of the 8,500 people reported dead or missing in Thailand [*Bagai et al.*, 2005; Kawata et al., online report, 2006] and widespread coastal destruction. Throughout this province, most of the fishing villages and their associated ecological environment were completely destroyed; many cultural landmarks suffered partial or total destruction. The largest tsunami runups (11 to 14 m) and destruction in Phang Nga province were observed near Khao Lak [*Tsuji et al.*, 2006] (see also A. Siripongse, Investigation and risk evaluation on tsunami disaster and suggestions on monitoring and prevention of tsunami, in *A First Report Under the Project: Investigation for Reclamation of Natural Resources and Environment by Chulalongkorn University*, submitted to the Ministry of Natural Resources and Environment, Thailand, 2005) (hereinafter referred to as Siripongse, submitted manuscript, 2005) on a 20 km stretch of shoreline that includes several popular beaches and resorts (Bahn Khao Lak, Nang Thong, Bang Niang, Pa Ka Rang, and Pak Tawib; from south to north in Figure 3, in the Khao Lak area). Damage to tourist

resorts, residential areas, and commercial buildings was widespread. A number of pictures and personal video recordings made in this area show that, after the initial ocean withdrawal, a large bore appeared, maybe reaching up to 8 m in height, and propagated as an almost straight line front approaching the Khao Lak beach and causing large runup. The second most impacted area in Thailand was the island of Phi Phi, which is located in Krabi province, 80 km east of the southern tip of Phuket (Figure 5; 98.8°E, 7.8°N). Phi Phi island suffered 15% of the fatalities reported in Thailand, when up to 6 m waves submerged a highly populated, narrow and low-lying sand isthmus (∼100–1,000 m wide and 2–2.5 m elevation), connecting two mountainous headlands between Tonsai bay (south coast of Phi Phi island) and Lohdalum bay (north of Phi Phi island). Eyewitnesses reported that waves hit the sand isthmus from both bays, first from the north side of the island, and a few minutes later from the south side; this was confirmed by personal pictures and video recordings (SEATOS, Sumatra earthquake and tsunami offshore survey, Cruise Report, 2005, http://www.oce.uri.edu/seatos/report.html) (hereinafter referred to as SEATOS, online report, 2005). Finally, Phuket Island was the third region of Thailand to be severely impacted by the tsunami, although it was much less heavily devastated than the Khao Lak area, and only locally, suffering 5% of the total fatalities in Thailand. A 5.5- to 6-m-high wave hit the western coast of the island, causing large runups (up to 10 m; Figure 3) and major damage, particularly at Kamala and Patong beaches. This resulted in 9% of the fatalities suffered in Thailand, with Kamala beach experiencing the most significant loss of life on the island. Destruction was widespread in Patong Beach, where not a single property escaped damage and eyewitnesses reported at least a 2-m-high surge that lasted for well over an hour, following the initial withdrawal.

[4] To better understand the large runups and destruction observed in coastal Thailand, and in view of the likelihood of similar future events occurring in the region (large earthquakes with M_w = 7.8–9.0 have occurred in 1797, 1833, 1861, 1881, 1907 and 1941 along this plate boundary [*Lay et al.*, 2005]), in this study, we perform detailed numerical simulations of tsunami runup and impact along the coast of Thailand for the 12/26/04 event. In earlier work [*Grilli et al.*, 2007], using a state-of-the-art Boussinesq model of tsunami generation, propagation, and runup, we had iteratively calibrated and validated a tsunami source for this event by comparing tsunami predictions with observations made at tide gauges in the Indian Ocean and the Andaman Sea, and JASON-1 satellite altimeter data measured in deep water. Here further model simulations are performed with a much finer regional grid defined over a smaller geographic area, using highly resolved bathymetric and topographic data in coastal Thailand. Specifically, the objectives of this study are to simulate: (1) runups over the whole Andaman coast of Thailand, where most post-tsunami field observations were made [*Tsuji et al.*, 2006; *Choi et al.*, 2006; Kawata et al., online report, 2005; Siripongse, submitted manuscript, 2005]; and (2) the sequence of events, at locations where these are available from eyewitness reports [e.g., *Papadopoulos et al.*, 2006]. We will show that our simulation is robust, in the sense that it explains most of the observed features of the tsunami along the Andaman Coast of
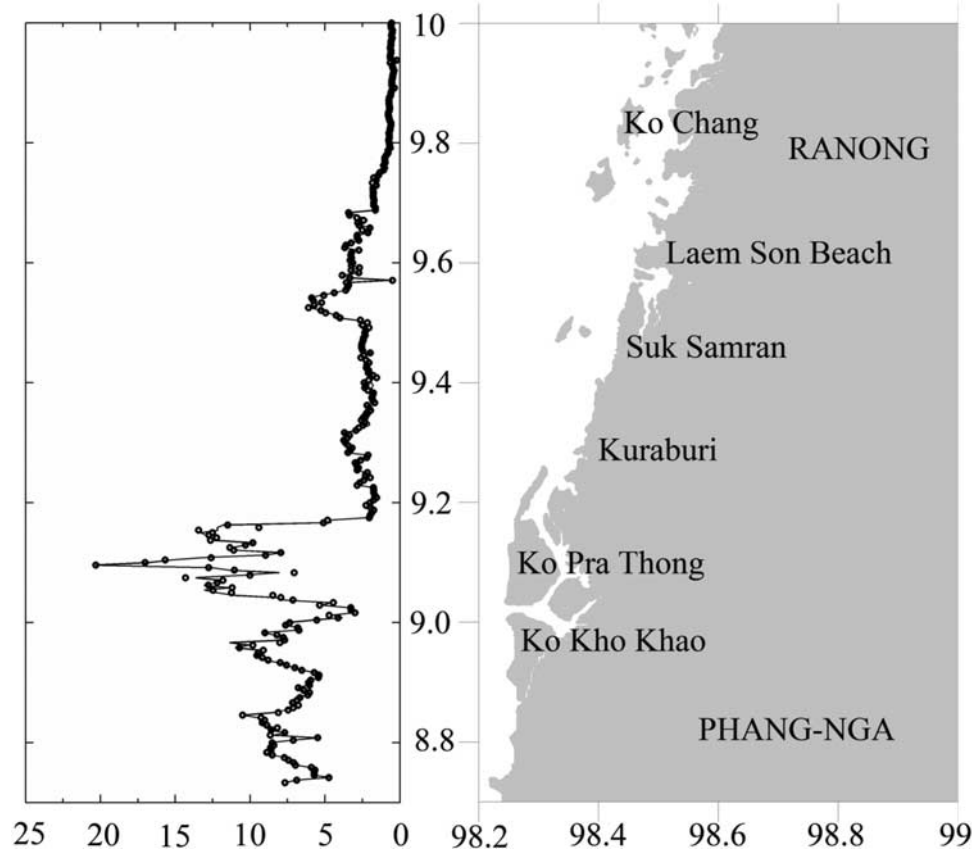
Figure 2. Simulated runup over the Andaman coast of Thailand in the north coast, Ranong province. The simulated runups are plotted along the coast. Solid lines are derived from the fully nonlinear Boussinesq simulation while circles indicate results of the Nonlinear Shallow Water (NSWE) model, neglecting frequency dispersion. Runup height is defined as the maximum surface elevation at the last inundated point of the initial topography.

Thailand, without these having been used to calibrate the tsunami source. Once these objectives are reached, we will use our validated synoptic predictions of tsunami impact in Thailand to globally analyze the event, including in areas where no observations were made. We will thus assess which areas may be safe or most likely vulnerable to future tsunamis in the region.

2. Overview of the Sumatra Fault Tectonics

[5] The relative motion between the Indian and Sunda Plates is on the order of 4 cm per year in direction 20°N while, between the Australian and Sunda plates, it is on the order of 5 cm per year in direction 8°N [*Socquet et al.*, 2006] (Figure 1). The 26 December 2004 $M_w \simeq 9.3$ megathrust earthquake [*Stein and Okal*, 2005] was a consequence of strain accumulated in the Indian/Sunda junction, some of which had not experienced a large earthquake for the past 150 years or so. Recent large events in the region include $M_w \sim 8.4$ in 1797, $M_w \sim 9$ in 1833, and $M_w \sim 8.5$ in 1861, for the Australian/Sunda boundary, and weaker $M_w \sim 7.9$ events for the Indian/Sunda boundary in 1881 and 1941 [*Lay et al.*, 2005]. This unbalanced partition of past earthquake magnitudes and recurrence times between the two plate boundaries indicates that larger strains had accumulated in the Indian/Sunda boundary prior to the

26 December 2004 event, and explains both the epicenter location at the junction between the subducting Indian and Australian plates and the overriding Eurasian plate (Burma and Sunda subplates) and the northward rupture propagation, where most of the aftershocks were recorded along a ~1300 km arc of the Andaman trench [*Lay et al.*, 2005]. The 28 March 2005 $M_w = 8.7$ event was a second large megathrust earthquake that occurred farther south, liberating additional strain on another stretch of the Australian/Sunda boundary and generating a small tsunami, locally causing a 4 m runup near the Islands of Nias. Finally, more recently, on 17 July 2006, a $M_w = 7.7$ earthquake occurred off southwest Java, liberating some more strain even further south along the same plate boundary and causing a devastating tsunami along 150 km of Java's coastline.

3. The 26 December 2004 Earthquake and Tsunami Events

[6] Before witnessing this event, scientists analyzed tsunamis generated by small-scale seismic ruptures as instantaneously triggered. This was a fairly good approximation because, for small rupture propagation times, the delay between tsunami time of triggering by coseismic bottom motion, and actual fault rupture was generally negligible as compared to travel time to the nearest coasts
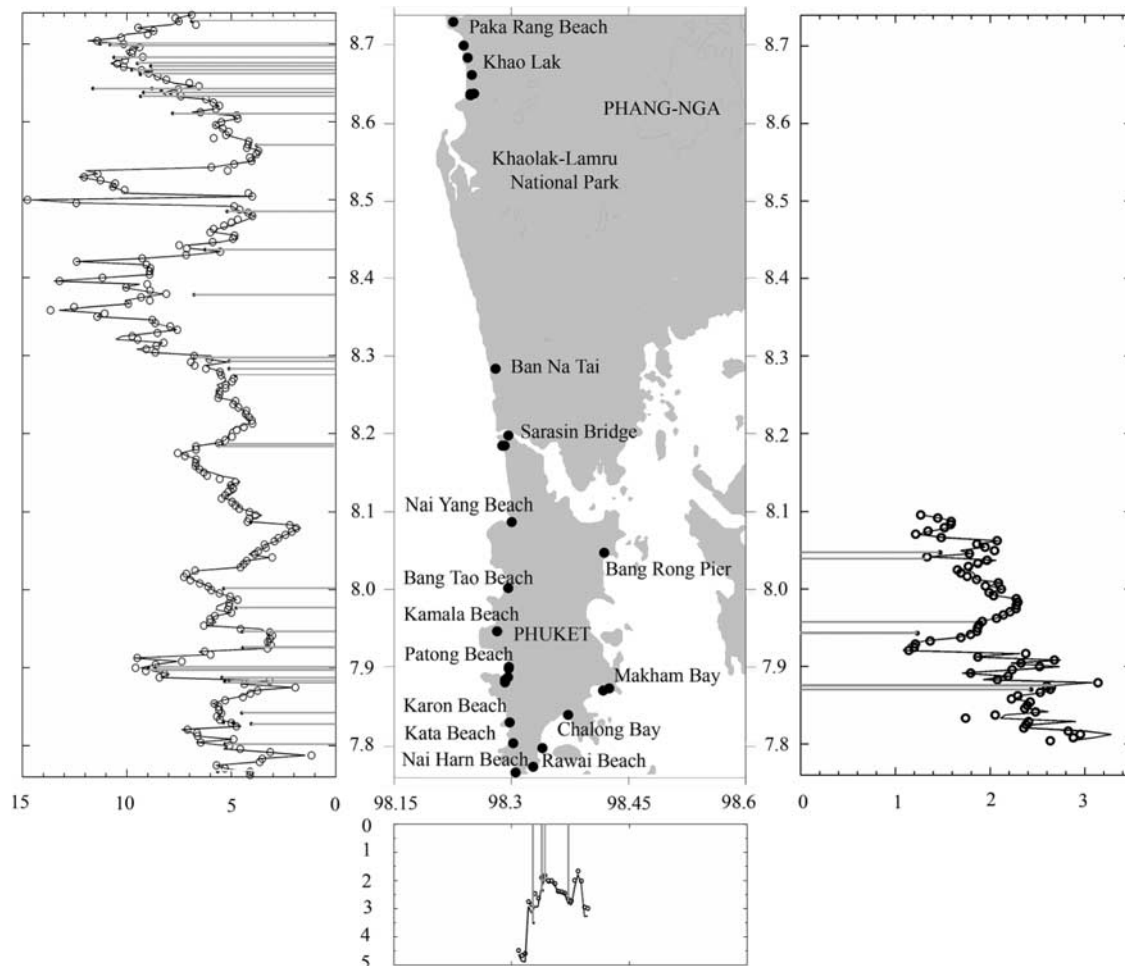
Figure 3. Same as Figure 2 for the Central Coast from Phang Nga province (Khao Lak) to Phuket island province; All (58) observed runup heights and locations (given in Table 2) are indicated by gray bars.

(e.g., the 16 November 1999 Vanuatu earthquake and tsunami [*Ioualalen et al.*, 2006]).

[7] The large size of the ruptured area of the 26 December 2004 event, however, raised many questions regarding the relationships between rupture speed and tsunami modes and timing of triggering by coseismic bottom motion. As far as past large-scale earthquakes and derived tsunamis, none were sufficiently well observed (through seismic and hydrographic networks) to initiate a comprehensive study of these relationships. The 26 December 2004 event is a milestone in this respect, because of its widespread observation with a sufficiently comprehensive and dense network to initiate such studies.

3.1. Summary of Earthquake Mechanism

[8] The earthquake occurred at 0h58′53″ UTC off the northern coast of Sumatra, Indonesia, at 95°51′, 3°25′ (Figure 1). The earthquake was measured in great detail over the Indian Ocean basin, using seismographs and GPS stations. Seismic inversion models [*Ammon et al.*, 2005; *Bilham et al.*, 2005; *Lay et al.*, 2005] indicate that, for about 500 s, the rupture propagated approximately northward from the epicenter, along 1,200–1,300 km of the Andaman-Sunda trench (with an average rupture speed of 2.5–3 km/s), causing up to ∼6 m of bottom subsidence and ∼10 m of

uplift over a region 100–150 km wide across the subduction area. According to *Bilham* [2005], up to 10 m uplift and subsidence were generated by the earthquake elastic rebound, offshore of Banda Aceh (northern tip of Sumatra). Seismic inversion and GPS records further indicate that fault slip was not homogeneous along the ruptured area varying between 15 and 25 m, with a gradual decrease northward from the epicenter [*Vigny et al.*, 2005]. (See *Grilli et al.* [2007] for a more detailed overview of rupture and bottom processes.)

3.2. Tsunami Observations

[9] Many real time observations of the tsunami were made in the Indian Ocean, perhaps so extensively for the first time owing to recent progress in observational techniques. Thus data are available from many tide gauges [*Merrifield et al.*, 2005; *Nagarajan et al.*, 2006] (also Royal Thai Navy, http://www.navy.mi.th/hydro/tsunami.htm, 2005) (hereinafter referred to as Royal Thai Navy, online report, 2005), a few satellite altimeters [e.g., *Gower*, 2005; *Smith et al.*, 2005], and a satellite Multi-angle Imaging Spectro-Radiometer (MISR) [e.g., *Garay and Diner*, 2007]. The very large extent of the ruptured area and large associated tsunami that was generated also contributed to their easier detection over a large domain. Beside these
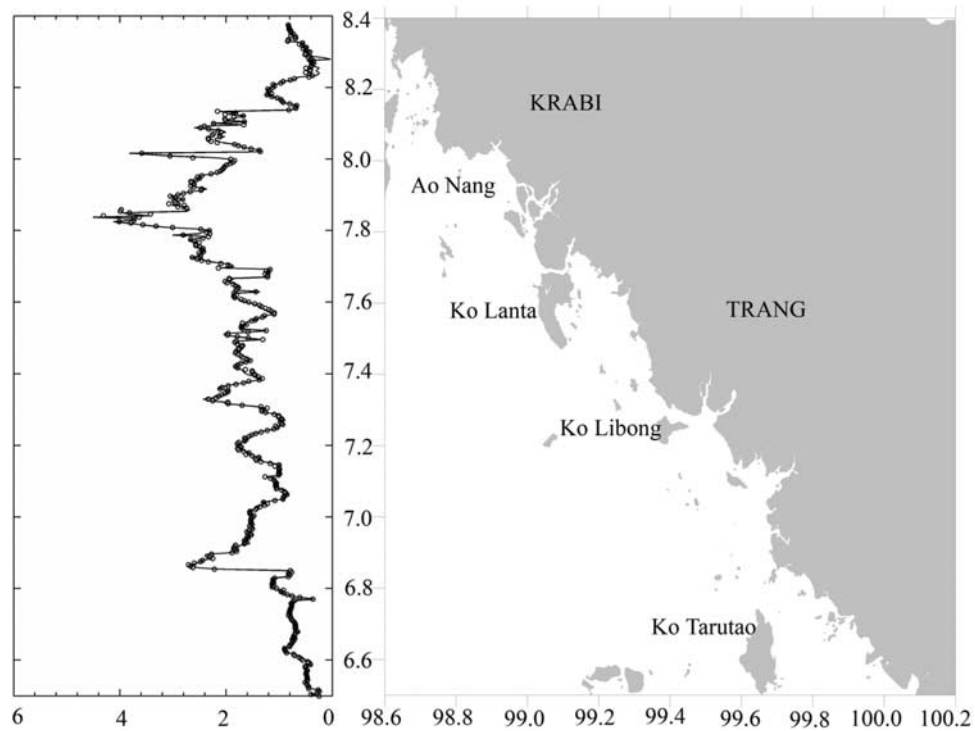
Figure 4. Same as Figure 2 for the south coast, for Krabi, Trang, and Satun provinces.

instrument records, numerous post-tsunami field surveys were made over the whole Indian Ocean basin [e.g., *Tsuji et al.*, 2006; *Choi et al.*, 2006; Kawata et al., online report, 2005; Siripongse, submitted manuscript, 2005]. This large amount of nonseismic data has helped better characterize the earthquake through constraints provided by the associated tsunami, such as arrival time of successive waves at tide gauges and along satellite transects.

[10] Thus, in our earlier work, we used many hydrographic data sets, including amplitude, timing, periodicity and sequence, of tsunami waves measured by various instruments, to iteratively develop and calibrate parameters of a multisegment coseismic tsunami source for the 26 December 2004 event [*Grilli et al.*, 2007] (Figure 1). The two main data sets used in this calibration are detailed below.

[11] The first data set consists of digital tide gauge or point surface elevation records. Most of these are tide gauges that are part of the Global Sea Level Observing system (GLOSS) network, monitored by the Joint Technical Commission for Oceanography and Marine Meteorology (JCOMM). Tide gauges that were used in the source calibration are located in Hannimaadhoo, Male and Gan (Maldives), Colombo (Sri Lanka), Diego Garcia (British Territory) and Cocos Island (Australia). UHSLC provides digital tide residuals, which can be directly compared with the simulated time series. A discussion of the tsunami signal detected by the tide gauges, including arrival times and sequences of tsunami waves, was given by *Merrifield et al.* [2005]. Additional tide gauges operated in Thailand were used, particularly that at Taphao-Noi (Royal Thai Navy, online report, 2005). Finally, a depth sounding record made a mile off Nai Harn Bay near the southwestern end of Phuket Island, onboard the yacht Mercator, in 12 m of water, was used that showed the arrival of three main waves over a duration of 35′.

[12] The second data set is the sea level anomaly detected by JASON-1's satellite altimeter, which happened to cut
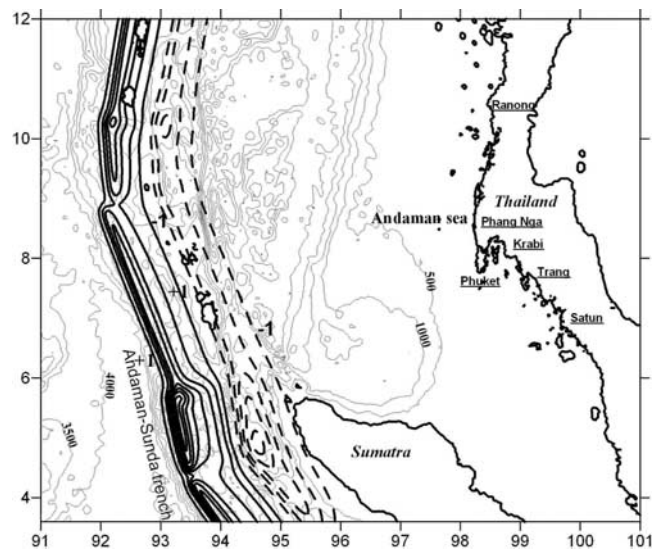

Figure 5. Initial surface elevation for tsunami source developed by *Grilli et al.* [2007] on the basis of five *Okada* [1985] dislocation segments (S1–S5; Table 1), in the fine computational grid. Continuous lines represent uplift and dashed lines represent subsidence, both at 1 m contour intervals in the range −5 to +8 m. The background bathymetry is plotted in grey at 500 m contour intervals. The six exposed provinces of the Andaman coast of Thailand are underlined.

across the evolving tsunami wave pattern in a north-south direction approximately 2 hours after the earthquake, during cycle 109 of pass 129 [*Gower*, 2005; *Smith et al.*, 2005]. *Grilli et al.* [2007] calculated the sea level anomaly over a diagonal transect in the Indian Ocean by subtracting measurements made during the earlier cycle 108 from cycle 109; they corrected for the travel speed of the satellite in their comparison with model results. Phenomena other than the tsunami may affect sea surface anomaly and cause errors, such as the internal and wind-forced variability of the ocean but, at relatively low latitudes such as here, the dominant timescales derived from basin-wide eddies are much larger than the period between two satellite cycles (around 10 days). Still, the obtained signal was noisy, maybe because of the relatively small Bay of Bengal basin, which may locally yield higher variability; thus the discrepancy between two cycles can be on the order of 20%, with or without a tsunami signal. Nevertheless, considering its magnitude (up to 1.20 m from peak to trough), the tsunami signal can be clearly identified in the records.

[13] A third data set, used here but not in the tsunami source calibration, consists in the runup values measured during post-tsunami field surveys made along the Andaman coast of Thailand [*Tsuji et al.*, 2006; *Choi et al.*, 2006; Siripongse, submitted manuscript, 2005]. Mostly densely populated areas, however, were surveyed, such as resort beaches in Khao Lak, Phuket, and Phi Phi island. Again it is one purpose of this work, through model simulations, to provide a synoptic and complete picture of tsunami impact in Thailand, including at locations where measurements were not made, and try to identify regions vulnerable to future tsunamis, independent of the density of the population. Such information would help in future regional development plans that might be considered.

[14] *Grilli et al.* [2007] performed model simulations using a $1' \times 1'$ grid (and 1.2 s time step), in a computational domain covering the entire Bay of Bengal, the Andaman Sea, and part of the Southern Indian Ocean (from $72°$ to $102°$E in longitude and from $13°$S to $23.5°$N in latitude). They simulated runups only at key locations (Banda Aceh in Indonesia, Khao Lak in Thailand), where the tsunami was most destructive, and favorably compared these with observations. In the present work, we use a finer $0.25'$ grid (with a 0.5 s time step), starting west of the northern tip of Sumatra and covering the Andaman sea up to the northern coast of Thailand, i.e., from $91°$ to $101°$E in longitude and from $3.6°$N to $12°$N in latitude (Figure 5).

4. Tsunami Simulations

[15] Numerical simulations of tsunami coastal impact require three components: (1) a source, reflecting the known geology and seismology of the event; (2) ocean bathymetry and coastal topography, and (3) a tsunami propagation and runup model, representing the relevant physics.

[16] Here we simulate tsunami propagation and inundation with FUNWAVE, a Boussinesq water wave model developed at the University of Delaware [*Wei and Kirby*, 1995; *Wei et al.*, 1995]. The model is fully nonlinear and dispersive, retaining information to leading order in frequency dispersion $O[(kh)^2]$ and to all orders in nonlinearity a/h (where k denotes an inverse wavelength scale, a a

wave amplitude, and h a water depth). FUNWAVE includes bottom dissipation and wave breaking, without which the wave would artificially amplify at the coast, and allows for land inundation through a moving shoreline algorithm [*Chen et al.*, 2000; *Kennedy et al.*, 2000], which has been fully validated for short-wave shoaling, breaking and runup. FUNWAVE has been calibrated to provide a stable model for tsunami runup, and has been successfully used to conduct various regional landslide tsunami case studies, including propagation and runup [e.g., *Day et al.*, 2005; *Ioualalen et al.*, 2006; *Watts et al.*, 2003; *Waythomas and Watts*, 2003]. (The combination of this calibrated version of FUNWAVE and TOPICS, which initializes various tsunami sources directly into it is referred to as GEOWAVE.) A more detailed description of FUNWAVE can be found in Appendix A and in work by *Kirby* [2003].

[17] Fully nonlinear Boussinesq models typically have an advantage over models based on the nonlinear shallow water equations (NSWE) in that they allow for the representation of both the slow accumulation of propagation effects due to frequency dispersion as well as for the accurate depiction of wave crest evolution during the final stages of shoaling and wave breaking. *Grilli et al.* [2007] have shown that the westward propagation of the tsunami wave during the Indian Ocean event was affected by dispersion to a significant degree. Below, however, we will show that the eastward propagation of the tsunami toward Thailand only exhibits weak dispersive effects, thus somewhat lessening the need for a model such as FUNWAVE, as compared to a more classical NSWE model. Nevertheless, FUNWAVE is retained here as the computational framework since both its energy dissipation, through bottom friction and breaking, and moving shoreline, algorithms have proved to be accurate for simulating tsunami runup and inundation [*Watts et al.*, 2003; *Ioualalen et al.*, 2006]. Note that the retention of nonlinear effects beyond the usual order in weakly nonlinear Boussinesq models is crucial for the correct modeling of shoaling solitary wave crests [*Wei et al.*, 1995], and hence is important for the correct modeling of tsunami-induced shoreline inundation.

[18] The version of FUNWAVE used in this study is implemented over a Cartesian coordinate grid and does not take into account Coriolis effects. However, these effects are not likely to be crucial for our case study. This is because the main tsunami propagation of interest in this work is in the west to east direction, and thus we were able to confine our computations in a relatively narrow equatorial domain where Coriolis effects are not significant. Horizontal distances are corrected in the model grid, on the basis of the Earth's curvature at $7.5°$N. For nondispersive simulations performed for reference, using the NSWE approximation, we utilize the same model, but with dispersive terms turned off and all other physical features retained.

4.1. A Best-Fit Tsunami Source Solution

[19] Once the propagation model grid is set up, using the ocean bathymetry and topography (see section 4.2), the first step in the simulation process consists in iteratively refining and calibrating a tsunami source. This is done by comparing the predicted tsunami dynamics with direct observations of tsunami arrival time and surface elevations, wherever available. As discussed in section 3, a number of tide

Table 1. TOPICS Input Parameters and Outputs for Five Tsunami Source Segments in Figure 1[a]

Parameters	S1	S2	S3	S4	S5
			Input Parameters		
τ, s	60	272	588	913	1273
x_o	94.57°E	93.90°E	93.21°E	92.60°E	92.87°E
y_o	3.83°N	5.22°N	7.41°N	9.70°N	11.70°N
d, km	25	25	25	25	25
φ	323°	348°	338°	356°	10°
λ	90°	90°	90°	90°	90°
δ	12°	12°	12°	12°	12°
Δ, m	18	23	12	12	12
L, km	220	150	390	150	350
W, km	130	130	120	95	95
μ, Pa	4×10^{10}	4×10^{10}	4×10^{10}	4×10^{10}	4×10^{10}
			Output Parameters		
M_o (J)	1.85×10^{22}	1.58×10^{22}	2.05×10^{22}	0.61×10^{22}	1.46×10^{22}
λ_o, km	130	130	120	95	95
τ_o, min	24.77	17.46	23.30	18.72	18.72
η_o, m	−3.27; +7.02	−3.84; +8.59	−2.33; +4.72	−2.08; +4.49	−2.31; +4.60

[a]Given are: time delay of segment rupture from earthquake time τ (a 60-s rising time is added); longitude and latitude of segment centroid (x_o, y_o); the centroid depth d, the fault strike angle φ (clockwise from north); the fault rake angle λ (counterclockwise from strike); the fault dip angle δ with the horizontal plane; the maximum fault slip Δ; the segment length along and width across (L, W); and the medium shear modulous μ; the seismic moment M_o; the characteristic initial tsunami wavelength λ_o and period τ_o; and the characteristic tsunami trough and peak amplitudes η_o. Note that in the simulation, slip is maximum at the segments' centroid and drops by 50% at a radius of L from it. The total seismic moment of all five segments is $M_o = 7.55 \times 10^{22}$ or $M_w = 9.25$.

gauges and satellite transect records were available in the Indian Ocean for the 12/26/04 event, which have been used by various modeling teams to validate their tsunami simulations at the ocean basin scale [e.g., *Hirata et al.*, 2006; *Fujii and Satake*, 2007]. *Grilli et al.* [2007] similarly used the two data sets detailed before to calibrate their simulations and iteratively developed a tsunami source for this event, made of five separate segments (Figure 1), modeled as a classical dislocation source, combining slip and strike motions occurring on an oblique fault plane embedded in a semiinfinite elastic material [*Okada*, 1985]. Source parameters were initially specified on the basis of results of seismic inversion studies [*Ammon et al.*, 2005; *Bilham et al.*, 2005; *Lay et al.*, 2005]. Each segment's geometrical, geological, and seismological parameter values, as well as each segment's triggering time τ, were then iteratively refined by comparing tsunami predictions with observations at tide gauges and along JASON-1's satellite transect. Details are given by *Grilli et al.* [2007]. The final calibrated source that is also used in this work, shows an inhomogeneous slip distribution along the trench, ranging generally from 12 to 18 m, but with an asperity or location of maximum slip of 23 m, off Banda Aceh (see Table 1 for source parameter values). This distribution agrees well with predictions of seismic inversion models and GPS observations [*Ammon et al.*, 2005; *Bilham et al.*, 2005; *Lay et al.*, 2005; *Vigny et al.*, 2005]. With these parameters, the Okada source segments yielded up to 9–10 m bottom uplift on the western side of the trench, and 5 m subsidence on the eastern side (Figure 5).

[20] Although the calibrated coseismic tsunami source used in this work seems accurate enough to model the 12/26/04 event, it should be noted that *Okada*'s [1985] dislocation model only provides an idealized way to characterize a seismic rupture. In particular the medium is considered homogeneous (a serious approximation) and the amount of slip is uniform on the derived fault rectangles (Figure 1). (To avoid the latter perhaps unrealistic constraint, in our source, we applied a Gaussian slip distribution from the fault centroid, within each segment (Table 1).) Hence Okada's representation should be understood as the simplest way to comprehensively represent a coseismic tsunami source that takes into account most of the fault geometry. For our tsunami modeling purpose, there are at least three transfer functions that we cannot estimate, i.e., the relationship between (1) the initial seafloor deformation and free surface shape: like in most tsunami studies so far, we assumed that these are identical; (2) Okada's solution and the real rupture process, which is largely unknown; and (3) the seismic rupture speed of propagation and mode (and speed) of propagation of the tsunami triggering mechanism itself, which should be different because the overlying medium (so-called accretionary prism) has quite different properties than the deeper geologic strata where the earthquake occurs, and thus involves different inertial forces. These three aspects, all sources of error in the development of an accurate tsunami source, are likely to be the object of important future research efforts, allowing for a better representation of tsunami sources. It is, however, fair to mention that a more accurate representation in the future would also require observational networks that are far beyond those currently available, for example, seismometers, GPS stations, to constrain it.

4.2. Computational Domain

[21] To perform the source calibration simulations summarized above, *Grilli et al.* [2007] used a $1' \times 1'$ model grid for the entire Bay of Bengal, from 72° to 102°E in longitude and 13°S to 23.5°N in latitude. The grid was defined mainly on the basis of $2'$ resolution bathymetry and topography [*ETOPO2*, 2001] (but was supplemented in coastal regions near Thailand with more accurate bathymetric data digitized from maritime charts, as described below).

[22] Here tsunami simulations are performed using a finer $0.25' \times 0.25'$ grid, to study coastal tsunami impact along the Andaman coast of Thailand, where most of the damage and
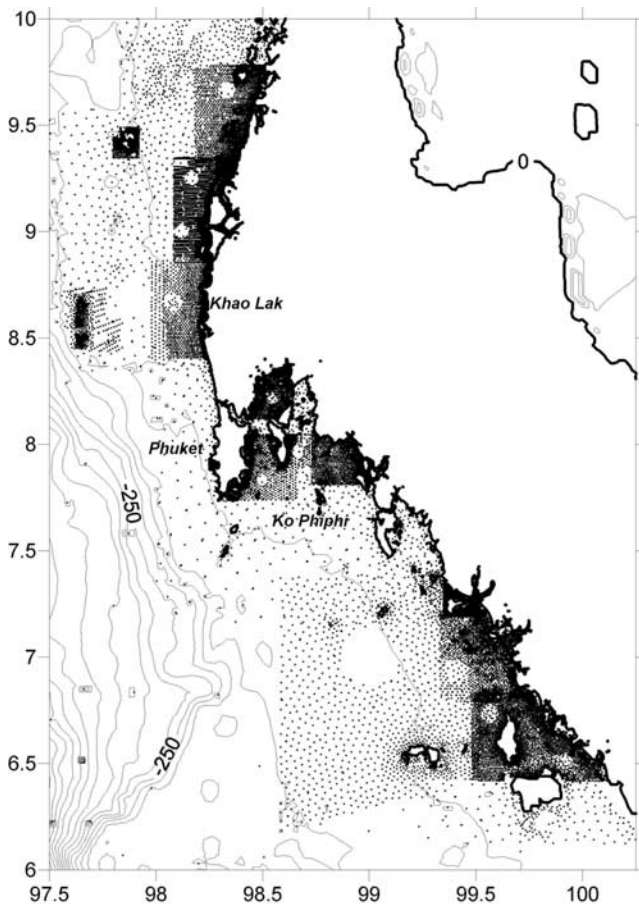
Figure 6. Location of bathymetric data points digitized from the Royal Thai Navy marine charts, along the western coast of Thailand. These data complement the 2′ ETOPO2 data, to construct the computational domain bathymetry (contoured at a 50-m interval in the background).

large runups were observed. This more detailed grid covers a smaller area off coastal Thailand (91°E–101°E, 3.5°N–12°N (Figure 5)), which includes most of the tsunami source developed by *Grilli et al.* [2007]. Only small parts of the first and fifth segments are not included in Figure 5; this does not affect tsunami propagation in the study area, which is mostly west to east. The grid bathymetry is again specified on the basis of ETOPO2 data, except in coastal Thailand, from Ranong to Satun, where higher-resolution data are used (Figure 6), allowing us to construct an accurate grid, both on land and sea, and truly compute nearshore tsunami propagation with our model at a 0.25′ resolution (about 460 m at these latitudes). These nearshore data were obtained from a composite approach using elevations from NASA's Space Shuttle Radar Topography Mission (http://srtm.usgs.gov/index.html, 2004) for the land area, on a 30 m resolution, and digitized maritime charts for the ocean area (Royal Thai Navy, Hydrographic Department maps at 50 m resolution, overlaid onto the 1:20,000 scale administrative boundary GIS; ESRI Thailand, Co. Ltd.; Figure 6). These two coastal data sets allow 15 and 9 observations between two grid points for the topography

and bathymetry respectively, avoiding any interpolation. The map projection rectification was verified and adjusted, wherever needed, using up to two ground control points per square kilometer. Figure 7 shows in the background some isobaths of the finer computational grid, for part of Figure 6 domain. Finally, we removed ETOPO2 bathymetry and topography along the Andaman coast of Thailand and replaced them by the above-cited more accurate data. Then the different data sets were merged and constrained by each other and the computational domain was gridded with a linear triangulation method.

[23] Within the computational domain, the Cartesian grid is homogeneous in horizontal spacing. Consequently, the maximum error as compared to spherical coordinates that may occur in longitudinal distances, when moving away from the source and its median parallel (7.5°N), is on the order of 0.6%, which represents at most 3′ to 4′ in space and around 50 s in tsunami propagation time, assuming a mean depth of 2000 m offshore. Such values are fairly small and will only add a small uncertainty to the following results. In any case the sphericity error essentially vanishes for the Thai coastline, because it is centered at 7.5°N where the grid error vanishes.

5. Runup and Flooding Simulations

[24] Figure 7 shows maximum tsunami elevations computed for coastal Thailand in the 0.25′ grid. Flooded areas can be seen on the figure by following the original coastline (0 m depth contour). The observed runup data were collected at 58 locations along the coast of Thailand by several international tsunami survey teams [*Tsuji et al.*, 2006; *Choi et al.*, 2006; Siripongse, submitted manuscript, 2005;]. *Tsuji et al.* [2006] describe the standard field survey techniques used for observing and recording runup heights, surveying inundated areas, as well as interviewing eyewitnesses.

5.1. Runups in Ranong, Phang Nga, and Phuket

[25] Figure 3 shows the continuous distribution of runups computed along the coast of Ranong, Phang Nga and Phuket provinces, as compared to all 58 observations available from *Tsuji et al.* [2006], Siripongse (submitted manuscript, 2005), and *Choi et al.* [2006] (data are given in Table 2). There is very good agreement between runup predictions and observations at all locations. The model also correctly reproduces the abrupt spatial variations in runup seen in observations (e.g., in Khao Lak, near Sarasin bridge, in Patong beach, in the southern coast of Phuket island). A 0.92 correlation coefficient is found, between observations and predictions (Table 3 for grid with $\Delta = 0.25′$). At the measured locations, observed runups range from 1.47 m to 11.29 m (mean: 6.11 m; s.d.: 2.71 m). Simulated runups range from 1.76 m to 10.30 m (mean: 6.05 m; s.d.: 2.61 m) and in general do not systematically underpredict or overpredict observations. The linear regression of runup simulations to observations (forced through the origin) has a slope of 0.97 (Figure 8). In the finer grid, the root-mean-square (RMS) error (a.k.a. model skill)

$$\varepsilon = \sqrt{\frac{\sum_i \left(r_{oi} - r_{pi} \right)^2}{n}} \qquad (1)$$
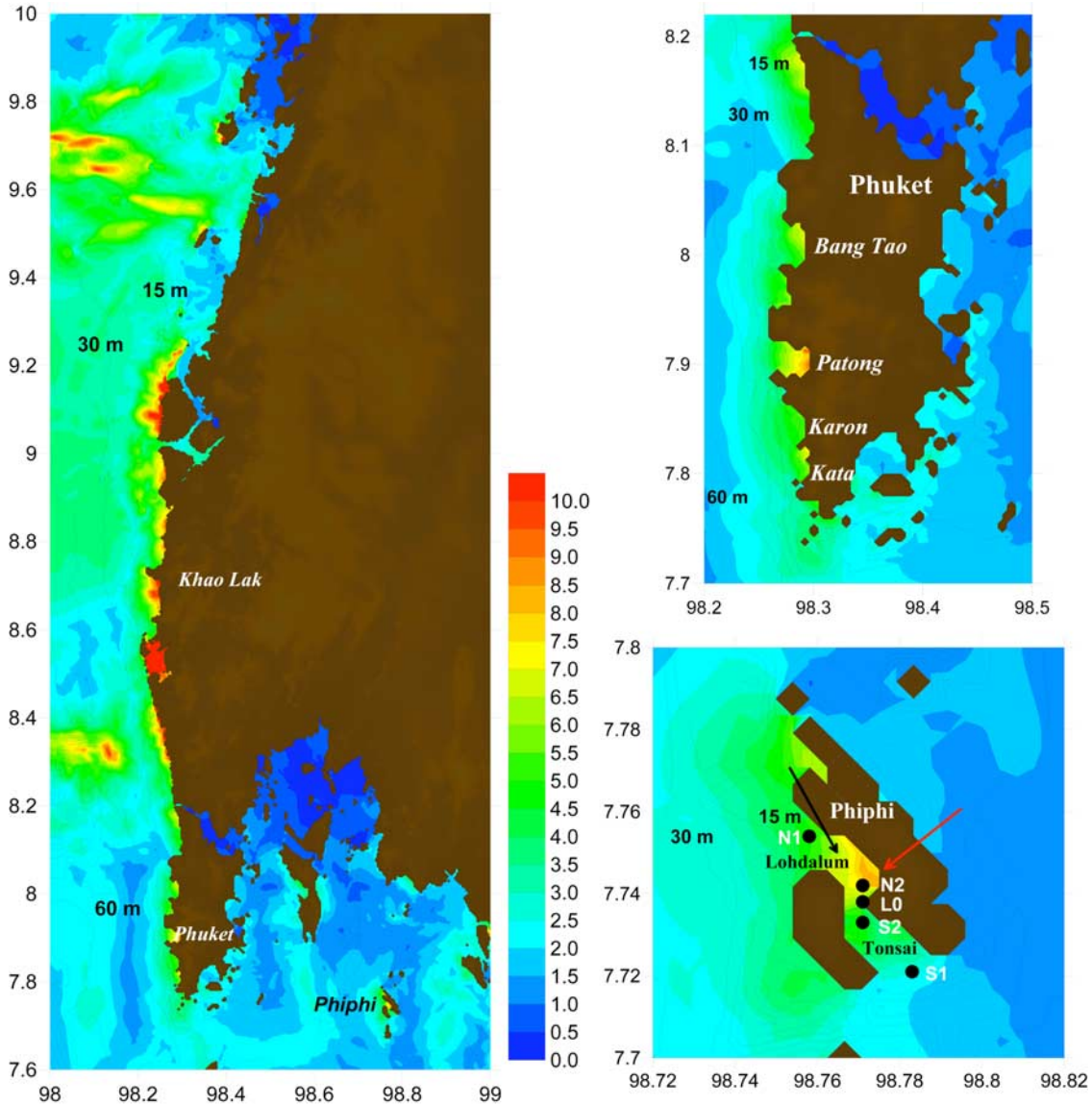
Figure 7. Maximum surface elevations (color-coded in meters) computed at any time in the $0.25'$ grid, along the (left) Andaman, (top right) Phuket, and (bottom right) Phi Phi islands. The bathymetry isolynes are shown in the background, making flooded areas visible. For Ko Phi Phi, simulated surface elevation time series are shown in Figure 14 for locations N2, N1, L0, S1, and S2. Arrows indicate the approximate location and direction of pictures taken during tsunami arrival (Figures 9, 10, and 11.)

is $\epsilon = 1.05$ m, or about 17.24% of the observed mean, the determination coefficient

$$R^2 = 1 - \frac{\sum_i \left(r_{oi} - r_{pi}\right)^2}{\sum_i \left(r_{oi} - \overline{r_o}\right)^2} \qquad (2)$$

is $R^2 = 0.85$ and keeps the same value for the linear fit in Figure 8 (i.e., 85% of the variance is explained by the model), and the norm

$$L^2 = \sqrt{\frac{\sum_i \left(r_{oi} - r_{pi}\right)^2}{\sum_i \left(r_{oi}\right)^2}} \qquad (3)$$

is $L^2 = 0.16$. The low ε and L^2, together with the high R^2 values, confirm the accurate prediction of the runup distribution along the coast in the grid with $\Delta = 0.25'$. All statistics were based on results obtained at the model grid point closest to each observation; no attempt at interpolation was made that might have further increased model skill.

[26] The high skill of runup predictions indicates that model results truly reflect, and thus can be used to better understand, tsunami impact as it occurred in Thailand during the 12/26/04 event. A sequence of simulated tsunami waves, arriving between Khao Lak Lamru and Pa ka Rang Beach, is shown in Figure 9, which illustrates tsunami propagation processes that can be both simulated and understood through modeling. We see that, 135 min after the earthquake, the incoming tsunami front gradually

Table 2. Observed Runup r_o and Predicted Runup r_p Along the Andaman Coast of Thailand for the 0.25′ Computational Grid[a]

Latitude or Longitude	r_o, m	r_p, m	Latitude or Longitude	r_o, m	r_p, m
7.7669°N	5.65	4.21	7.8420°N	4.49	5.43
7.8025°N	5.30	6.08	7.9000°N	8.96	9.33
7.8293°N	4.92	5.00	7.9260°N	4.44	3.39
7.8826°N	5.31	3.45	7.9770°N	4.76	5.71
7.8838°N	5.09	3.84	8.0870°N	4.07	3.83
7.8874°N	5.44	8.25	8.1850°N	5.31	6.40
7.9003°N	8.61	9.28	8.2740°N	4.80	5.45
7.9465°N	4.47	3.37	8.2930°N	5.10	5.52
8.0019°N	5.36	5.97	8.2970°N	6.77	6.20
8.0868°N	4.07	3.73	8.3780°N	6.78	8.53
8.1841°N	5.58	6.63	8.4360°N	6.25	6.42
8.1860°N	5.41	6.14	8.4850°N	5.19	4.54
8.1990°N	5.36	5.12	8.5700°N	3.80	4.14
8.2833°N	5.10	5.98	8.6110°N	7.80	6.18
8.6402°N	8.35	7.90	8.6330°N	9.34	7.92
8.6611°N	9.35	8.80	8.6370°N	7.91	8.27
8.6667°N	8.80	9.24	8.6380°N	9.20	8.23
8.682°N	10.62	9.72	8.6430°N	11.62	7.39
8.7003°N	11.29	10.30	8.6430°N	8.80	7.39
8.7291°N	6.90	7.46	8.6620°N	9.35	8.88
7.8702°N	2.43	2.66	8.6640°N	8.99	9.03
7.8729°N	2.67	2.63	8.6660°N	8.92	9.19
7.9432°N	1.23	1.79	8.6670°N	9.77	9.31
8.0475°N	1.47	1.76	8.6720°N	8.85	10.41
98.3280°E	3.50	3.03	8.6750°N	9.50	10.77
98.3397°E	2.35	2.12	8.6990°N	10.80	9.98
98.3725°E	2.75	2.82	7.9590°N	2.06	1.83
7.8280°N	4.04	4.86	8.0470°N	1.47	1.77
7.8300°N	5.38	5.08	98.3400°E	2.35	2.10

[a]Observed runup includes 58 data; see Figure 3 [*Tsuji et al.*, 2006; *Siripongse*, 2005; *Choi et al.*, 2006]. For computation grid, see Figure 8. The position is given in latitude or longitude.

refracts from an orientation of 340°N, near the 60 m isobath (Figure 7), to nearly 360°N (i.e., the northern part of the front is propagating faster than in the southern part), when it reaches the shore 20 min later causing wave focusing in this area. Prior to the tsunami front reaching shore, one clearly sees, by comparing the first two plots, that pieces of the shoreline have emerged, because of ocean withdrawal caused by the leading depression wave. By contrast, when the tsunami front impacts the shore, the third plot shows intense coastal flooding in some coastal areas. Additional results of simulations would show that the oblique incidence of the tsunami front would cause northward propagating reflected waves in some areas, that then rereflected off the Paka Rang Beach headland, leading to a combination of

waves that further increased runup. Some of the largest observed and modeled runups in Thailand indeed occurred in the Khao Lak region (Figure 3).

5.2. Runup on Phi Phi Island

[27] As discussed above, in Phi Phi island or so-called Ko Phi Phi, fatalities and destruction of buildings were well above 50%. This is in part because the tsunami hit the island without warning but also because the topography of the island, which had its highest inhabited area in a narrow and low-lying sand isthmus separating two headlands, acted as a death trap. The well-documented arrival and impact of the tsunami and the unusually complex local bathymetry and topography, make modeling the event at Phi Phi quite a challenge, from which we may learn valuable lessons regarding tsunami impact on island communities in general.

[28] The center of Phi Phi island is located at 7°45′N and 98°47′E, approximately 80 km east of the southern tip of the island of Phuket (Figure 7). The island has a butterfly shape with two headlands on the eastern and western sides (with a maximum elevation of 185 m), connected by a narrow sand isthmus, about 1.2 km long and 100–1,000 m wide, running west-east (Figure 10, top). Prior to the tsunami event, owing to its topography, most of the island's population and tourism infrastructures (hotels, resorts, guest houses, restaurants, shops, . . .) were located on the sand isthmus, which was thus densely built. Both supplies and visitors were transported to and from Phi Phi island by a ferry boat, which regularly sailed from Phuket and docked in a small harbor on the southern side of the sand isthmus. Phi Phi island typically had a population of 2,000–3,000 people, during peak holiday periods, half of these being tourists. On the morning of 12/26/04, because this was Sunday and weekly rentals expired, many tourists had fortunately already left the island on an earlier ferry, while tourists coming on the New Year vacation had not yet arrived. Many tourists, however were still packing in hotels and, particularly, in the large resort located on the northwest side of the sand isthmus (large buildings above the center of Figure 10, bottom).

5.2.1. Tsunami Arrival Sequence From Visual Evidence

[29] Two sequences of still pictures taken by eyewitnesses during the event are discussed in the following, that show both the arrival and impact of large tsunami elevation waves that hit Phi Phi island. Pictures were taken around 10h45′ local Thailand time, i.e., about 2h46′ after the earthquake started. On the basis of eyewitness reports,

Table 3. Comparison Between Observed and Modeled Runup Statistics Along the Andaman Coast of Thailand for Different Model Grid Resolutions Δ[a]

Δ	$\overline{r_o}$, m	σ_{r_o}, m	$\overline{r_p}$, m	σ_{r_p}, m	$\rho_{o,p}$	ε, m (Percent $\overline{r_o}$)	R^2	L^2
0.25′	6.11	2.71	6.05	2.61	0.92	1.05 (17.24)	0.85	0.16
0.5′			5.68	2.87	0.87	1.51 (24.77)	0.68	0.23
0.75′			6.10	3.60	0.80	2.16 (35.30)	0.37	0.32
1′			6.15	3.87	0.86	2.07 (33.85)	0.42	0.31
1.5′			4.62	3.19	0.79	2.45 (39.99)	0.19	0.37
2′			4.16	3.25	0.83	2.67 (43.74)	0.03	0.40

[a]Reported values include the mean observed runup $\overline{r_o}$, mean modeled runup $\overline{r_p}$, the standard deviations (σ_{r_o}, σ_{r_p}), the correlation coefficient $\rho_{o,p}$, the RMS error ε (in meters and in percentage of the mean $\overline{r_o}$) (equation (1)), the determination coefficient R^2 (equation (2)), and the L^2 norm (equation (3)).
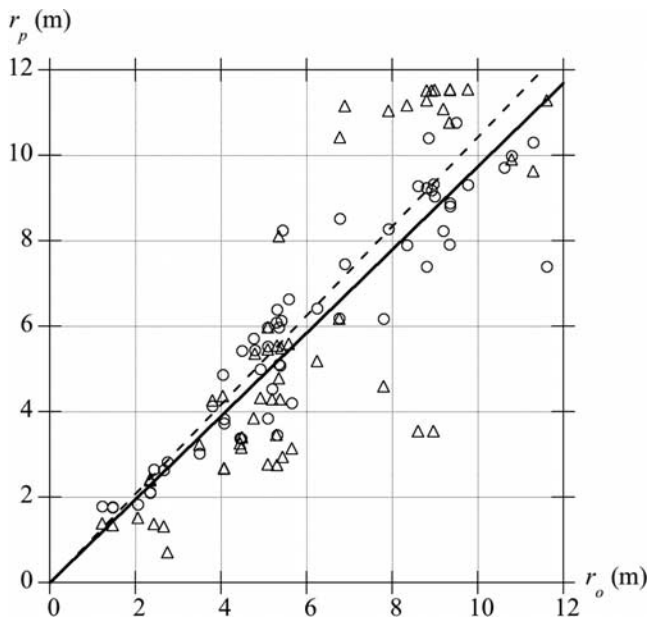
Figure 8. Observed r_o versus predicted r_p runups along the Andaman coast of Thailand (Figure 2). Simulations were performed with the Boussinesq model using ($\circ$) $0.25' \times 0.25'$ grid, or ($\triangle$) $1' \times 1'$ grid. The linear least squares fits, solid line through circles and dashed line through triangles, are forced through the origin.

people were largely unaware there had been an earthquake in the region, let alone a tsunami. A few inhabitants interviewed during two visits we made to Phi Phi in May 2005 (SEATOS, online report, 2005) reported having felt some vibrations but none had any clue a tsunami was coming. Most people on the island were having their normal activities, which took place mostly on the sand isthmus. Hence the tsunami toll on the island was particularly heavy in proportion to the population, with 1,300 reported dead or missing. As can be seen on Figure 10 (bottom) destruction was almost total in the middle part of the sand isthmus and on its western side, except for the solidly built resort floors located above the ground floor. On the north side of the middle part area of the sand isthmus, in particular, we were told none of about 300 well-built wood cottages were left standing, not even their foundation.

5.2.1.1. Pictures From the Hilltop

[30] The first set of pictures (Figures 11a–11e), was taken by Das Ehepaar J. T. and Caroline Malatesta, looking down and westward from the highest point on the eastern side of the island (viewpoint at 185 m above sea level marked by a red arrow in Figure 7). They had left for a hike earlier in the morning and first observed unusual wave activity in the northern bay of the island (a full account of their fateful morning can be found at http://www.magazine.wlu.edu/web/page/print/386.html):

[31] 1. "…Caroline pointed out to me that the water was changing color and withdrawing to the sea.", "…we noticed that the bay started receding, almost like a bathtub being drained. At first we thought it was low tide and were fascinated at how quickly the tide went out. However, then

it kept on going and going until the sea floor and coral reefs were exposed." "We were amazed that we could see rocks and coral reef exposed nearly 100 yards from the shore.", "We knew that low tide had generally been around noon so we found it odd that the water level was going down so early in the day…". They were apparently witnessing the arrival of a depression wave in the northern bay of the island (Figure 11a).

[32] 2. "About five minutes later, we saw a wave the length of the bay coming toward the shore." "We realized that it was big when we saw it pick up a speedboat as if it were a feather and just carry it all the way inland." This was the arrival on the north shore of the first large elevation wave in the tsunami wavetrain (Figures 11b and 11c).

[33] 3. "The water crashed into the shore and completely flooded the island. Palm trees were falling and people were screaming." This was the wave impacting the northeast side of the bay, reflecting off it and moving down the beach, in the manner of an edge wave, and heavily flooding the northwest side of the sand isthmus (Figures 11c, 11d, and 11e).

[34] Looking more closely at these pictures, we clearly see in Figure 11a, of flow of gray water exiting the Northern Bay, exposing rocks, and in Figure 11b, to the left, many rocks and shallows being exposed. Then, in Figure 11b (to the right), a wave as wide as the northern bay is approaching from the north, as a breaking bore, in a general southeast direction. In Figure 11c, this wave both floods and reflects off the northeastern side, then causes maximum runup on the northwestern side (Figures 11d and 11e). The "Belgian waffle" wave pattern seen in the lower part of Figure 11d is indicative of two intersecting (incident and reflected) wave trains. In Figures 11d and 11e, the tsunami floods the middle part of the sand isthmus and the large hotel resort on its northwestern side, and behind it, up to the second floor level.

[35] More pictures were taken after the arrival and impact of the first elevation wave in the Northern Bay. Figures 12a and 12b show the beginning of the arrival of a tsunami wave in the Southern Bay (lighter colored water), while flood water that accumulated on the north shore is starting to flow over the sand isthmus into the Southern Bay, carrying a lot of debris (brown water). In Figure 12a, we clearly see that both the middle part and western side of the sand isthmus were completely flooded, resulting in almost complete destruction in the middle and eastern part of the isthmus (Figure 10, bottom). In Figure 12b, the larger hydraulic head on the northern shore creates a strong debris flow into the Southern Bay, starting from the western side and moving down to the middle of the sand isthmus. Damage surveys confirmed these observations (upper parts of cottages from the northern shore were piled up on the southern shore; a large amount of debris were covering the harbor in the Southern Bay). The arrival of tsunami waves from the south and the simultaneous flow north-south through the sand isthmus, of water accumulated on the north shore by the first elevation wave, were both confirmed by eyewitnesses interviewed during our two visits to Ko Phi Phi; many small boats and people were reported to have been literally flushed from the northern into the Southern Bay. The tsunami that occurred in the Southern Bay, and caused additional destruction by moving eastward, was reported to also propagate in the
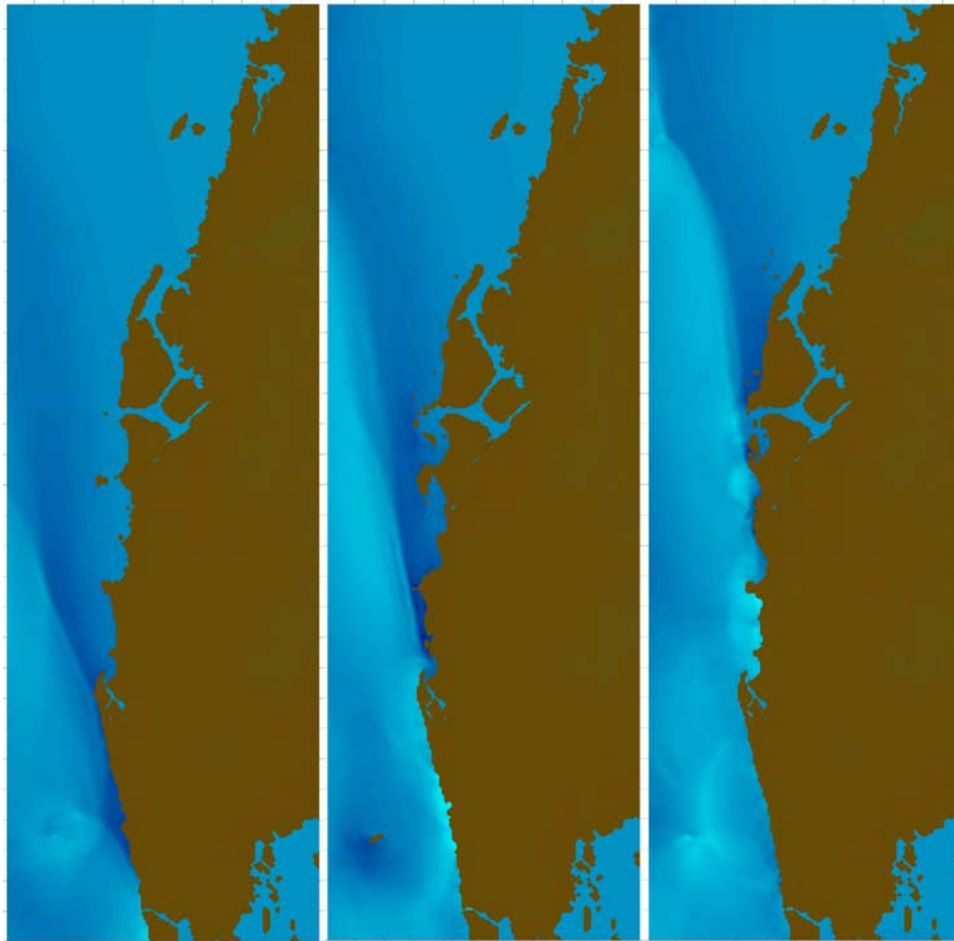
Figure 9. Sequence of simulated tsunami elevations (north of Phuket; Figure 3): (left) 135, (middle) 145, and (right) 155 min after the earthquake. The darker blue color represents depression waves while the lighter blue represents large elevation waves.

manner of an edge wave along the southern beach (not documented in this sequence of pictures). In Figure 12c, we see the effect caused in the southern harbor by an incoming depression wave, while water is still present in the north shore. Finally, Figure 12d shows an undular bore moving out of the Northern Bay (timing uncertain). This bore could be due to the combination of another depression wave arriving in the Northern Bay, with the elevation wave that has arrived shortly before in the south shore, causing a northward flow over the isthmus, because of their combined hydraulic head.

5.2.1.2. Pictures From Yacht *Gaultine III*

[36] Pictures in Figure 13 were taken from a yacht anchored near the east side of the northern bay, about 1 km from shore (marked by a black arrow in Figure 7). This picture sequence lasts for $\simeq 5'$, from the approximate time the water reached a minimum owing to the initial depression wave and hence covers the arrival of the first wave of elevation also seen in Figures 11b–11d. The sequence is consistent with our earlier discussion but provides an interesting viewpoint, particularly regarding wave height, since it was taken looking horizontally from about 3.3 m above local sea level, from the deck of the

Gaultine III yacht (a full account of these observations can be found at http://www.yachtaragorn.com/Thailand.htm).

[37] In Figure 13a two boats, "...*Gaultine III* and *Aragorn*, are spun in a counterclockwise eddy of the ebb coming off the beach...". It is clear here that the ocean is withdrawing, causing an ebb-like flow coming from the beach. Taken also during the first minute, Figure 13b shows the scene facing south, to the right of Figure 13a, with the beginning of the sand isthmus visible to the right of this picture. In both figures, one clearly sees that the reef is emerged and many large rocks are visible.

[38] Figures 13c–13g follow each other along the eastern side. Figures 13c–13f, taken during the third minute show a large breaking wave (bore whose backside we see) moving in a southeast direction, reflecting off the shore and starting to break backward. The wave appears to be 4–5 m high in the last two pictures: "...By this time, the wave must be 15 feet tall behind the cat...". In Figures 13e and 13f (blow up), we see the left leaning mast of one of the boats caught between the wave and the eastern shore.

[39] In Figure 13g, taken in the fourth minute, we see the same boat's mast as in Figure 13f, behind the catamaran, leaning right the other way. Behind and closer to shore, the

Figure 10. Pictures of Ko Phi Phi looking west (top) a few minutes before the tsunami arrival on 26 December 2004 (by Das Ehepaar J. T. and Caroline Malatesta, http://www.magazine.wlu.edu/web-page/print/386.html), and (bottom) destruction in the sand isthmus area after the tsunami hit, early 01/05 (by Ed Wardle).

main wave gets taller and clearly moves to the right. This is the beginning of the intense reflection seen in Figures 11c and 11d, causin an edge-wave-like propagation westward, parallel to the sand isthmus. In Figure 13h, to the right of 13g, we are looking directly south at the sand isthmus (the cell phone tower to the east of the sand isthmus is visible on the left of the picture) and we see a large wave is directly about to impact the beach: "...the wave is higher than the spit of land, as only first-story roofs are visible behind the wave. The motorboat in the foreground was able to escape...". Numerous roofs of one story buildings, likely the north shore cottages mentioned before, are barely visible above the wave. This stage approximately corresponds to Figure 11c.

[40] Figure 13i was taken during the fifth minute and "...shows the wave crest at its highest, covering your view of the second story windows in the hotel (resort) in back. The speedboat is getting out of there, and you can see by the lack of a wake on the dink that the water is about to turn to ebb again." This stage approximately corresponds to just before the stage of Figure 11d.

[41] Figure 13j, taken the morning after, looks south to the east of the resort. One can see the sand isthmus' elevation above MWL and that the island has been cleaned of many trees and its buildings, except for the large hotel resort to the right.

5.2.2. Runup Data

[42] Figure 11f was taken during our own field survey of Phi Phi and we see how high the water reached on the side of a large building belonging to the hotel resort located west of the sand isthmus, on the north shore, i.e., at midheight of the little roofs covering the entrance porches; the tip of one of these roofs emerging from the water can be seen on the left of Figure 11e. Although we did not have accurate surveying equipment, we estimated the midpoint of these roofs to be at 5.5–6 m above sea level. In Figure 11e, we see runup might even have been larger behind the resort, owing to the presence of the hill.

[43] A Japanese survey team (K. Harada, The December 26, 2004 Sumatra earthquake tsunami, Tsunami field survey around Phuket, Thailand, 2005, http://www.drs.dpri.kyoto-u.ac.jp/sumatra/thailand/phuket survey e.html, Research Center for Disaster Reduction Systems, Disaster Prevention Research Institute, Kyoto University, Japan) reported two maximum runup measurements made on the northern shore of the sand isthmus of Phi Phi. One measurement of 5.32 m, 62 m from shore at the westward extremity, referred to as "second floor of hotel," is consistent with our own observation at the resort hotel (Figure 11f). The other measurement of 6.89 m, 242 m from shore at the eastward extremity is a trace on a house wall in town, in the area first hit by the largest elevation wave (lower part of Figure 11c). The survey team suggests to correct these raw measurements by subtracting the tide levels in Phuket, which was maximum at 10 am local time on 12/26/04, at around 0.75–0.8 m above MWL.

5.2.3. Simulation Results

[44] Simulations in Figure 7 indicate that, on Phi Phi island, the highest waves (up to 7.5 m) occurred in the east of the northern bay (Lohdalum), and that the narrow sand isthmus between the two headlands was fully submerged at some point during the event. The largest wave elevations predicted on the east of the north shore correspond well to the reflection of the first elevation wave off this side of the island, seen in the two picture sequences discussed above. On the west of the northern bay, near the isthmus, simulated waves reached 6.5–7 m, which is very close to the measurement made by post-tsunami survey teams and our own observation.

[45] Figure 14 gives time series of surface elevation computed at points N1,N2,L0, S2 and S1 (from north to south in Figure 7). The sequence of simulated wave elevations indicates that, as reported by eyewitnesses and seen in the picture sequences discussed above, tsunami waves first arrived from the north, peaking at N1 then N2, and second from the south, peaking at S1 then S2. Before these first elevation waves occurred, we see that at N2, the initial depression wave reached the ocean bottom (3 m depth) at 2h31′, which stayed dry for about 5′, as reported by eyewitnesses and seen on pictures. The reef was emerged again at 2h54′ at N2 for about 6′, after the first elevation wave passed by. We see that, at N2, it took about 6′ for the elevation wave to peak at about 7 m, from the time it started arriving, after the first period of reef emergence (about 2h36′ in Figure 14). This corresponds well to the 5′ picture sequence from the yacht *Gaultine III* discussed above. During the passage of the first elevation wave, we see that point L0, which is initially a land point on the isthmus (2.5 m elevation), was submerged at 2h40′ for about 6.5′, by up to 2.5 m of water, owing to waves coming from the north; this agrees with eyewitness reports and picture sequences showing that waves incoming from the north flowed over the narrow isthmus into the southern Tonsai bay (harbor side); this also agrees with the observed

Figure 11. Arrival of 26 December 2004 tsunami on Ko Phi Phi's north shore, at approximately 10h45′ local time, see from the hilltop viewpoint (red arrow in Figure 7). (a) Effect of the first depression wave on the north shore; (b) arrival of first large elevation wave on the north shore; (c) elevation wave runs-up northeast beach; and (d) elevation wave reflects off northeast beach and moves westward as an edge wave. (e) Maximum runup occurs on northwest beach. (f) Telltale of maximum runup on 5/9/05 (at ∼5.5−6 m above MWL). (Pictures 11a−11e were taken by Das Ehepaar J. T. and Caroline Malatesta, http://www.magazine.wlu.edu/web/_page/print/386.html; Figure 11f was taken by S. Grilli.)

direction and deposits of debris flows from north to south over the sand isthmus.

6. Model Sensitivity Analyses

[46] The iterative calibration of the tsunami source parameters (Table 1) used in the model [*Grilli et al.*, 2007] was not based on any observed runup values, but only on measured surface elevations at tide gauges and one satellite transect. Thus the good agreement in Figure 3 between simulated and observed runups provides an indepen-

dent validation of our modeling approach, which confirms that, at the selected spatial and temporal scales, the model adequately represents key physical processes at play during tsunami generation and propagation (i.e., source parameters, computational grid scale and associated bathymetry), but, more importantly, during runup (including shoreline motion, dissipation due to wave breaking, and reflection). Hence the numerical simulation is robust in the sense that all its parts are fully consistent with each other.

[47] It should be stressed, however, that runup measurements were all made along sections of the coast mostly

Figure 12. Continued from Figure 11. (a) West of north beach is flooded by first large elevation wave, up to second floor of buildings, arrival of tsunami at south beach harbor. (b) Flood caused by elevation wave flowing through the island's narrow sand isthmus, north-south into harbor, carrying debris. (c) Effect of first depression wave in the south beach harbor, while water is still present in the north shore; shown is accumulation of debris in the harbor. (d) Undular bore, moving northward off the north shore. (Pictures were taken by Das Ehepaar J. T. and Caroline Malatesta.)

deprived of small-scale bathymetric features, for which most of the control was due to tsunami propagation over the nearshore bathymetry. The 460 m grid size is still not adequate to represent runup processes owing to smaller-scale bathymetric or topographic features, if these become dominant. A sensitivity to model grid size is performed below, which confirms the adequacy of the 0.25′ grid to model measured runups and further discusses scale considerations.

6.1. Sensitivity to Grid Size

[48] The fact that runup predictions are in such a good agreement with observations, despite the still fairly coarse model grid size of ∼460 m, indicates that the magnitude of runups in the studied area should mostly be governed by processes occurring at larger scale, namely tsunami propagation and transformation over offshore bathymetric variations, and not by details of the coastal topography. To verify this hypothesis, we recalculated the runup variation along the Thai coastline in a series of gradually coarser model grids, up to a 2′ grid spacing (Table 3). The correlation coefficient between observed and predicted runups does not deteriorate significantly up to the 2′ grid (from 0.92 for 0.25′ to the lowest value of 0.79). This shows that, in part because the shoreline lacks significant tortuosity at these low latitudes, most of the runup variability along the coast is fairly well reproduced (in an order of magnitude sense) even in a coarse grid. However, for increasing grid spacing the RMS error ε, the determination coefficient R^2, and the L^2 norm all significantly deteriorate, suggesting that in the coarser grids, despite representing the magnitude of runup well, the model is unable to accurately predict runup at specific locations. Hence there is a large sensitivity of wave elevation computed at a particular site, to grid resolution. This sensitivity stresses the need to use a fine enough grid, with accurate bathymetric and topographic data, to perform detailed runup simulations. However, the question remains to know how fine a grid this should be.

[49] The trend exhibited in Table 3 for the RMS error, the determination coefficient and the L^2 norm show that the 0.25′ grid seems an optimal resolution, because all these basic statistics have uniformly reasonable values (whereas at coarser grid size one or the other do not, particularly ε and R^2) and, overall, R^2 indicates that 85% of the measured runup variance is explained by the model, which is quite a high value for such natural hazard simulations. Making the grid finer than 0.25′, on the other hand (which would significantly increase computational cost), might only slightly further improve those statistics, but would not likely provide significantly more useful information regarding the impact of the tsunami event in Thailand. Another analysis in support of our choice of resolution is given below.

[50] Starting with *Van Dorn* [1965], the longshore variability of tsunami runup has been shown, in the vast preponderance of cases, to closely follow a log-normal distribution. Recently, *Choi et al* [2006] examined tabulated runup observations for the 2004 Indian Ocean event and showed that observed values follow such a distribution. Previous studies have also demonstrated that modeled tsunami runup follows a log-normal distribution [*Choi et*
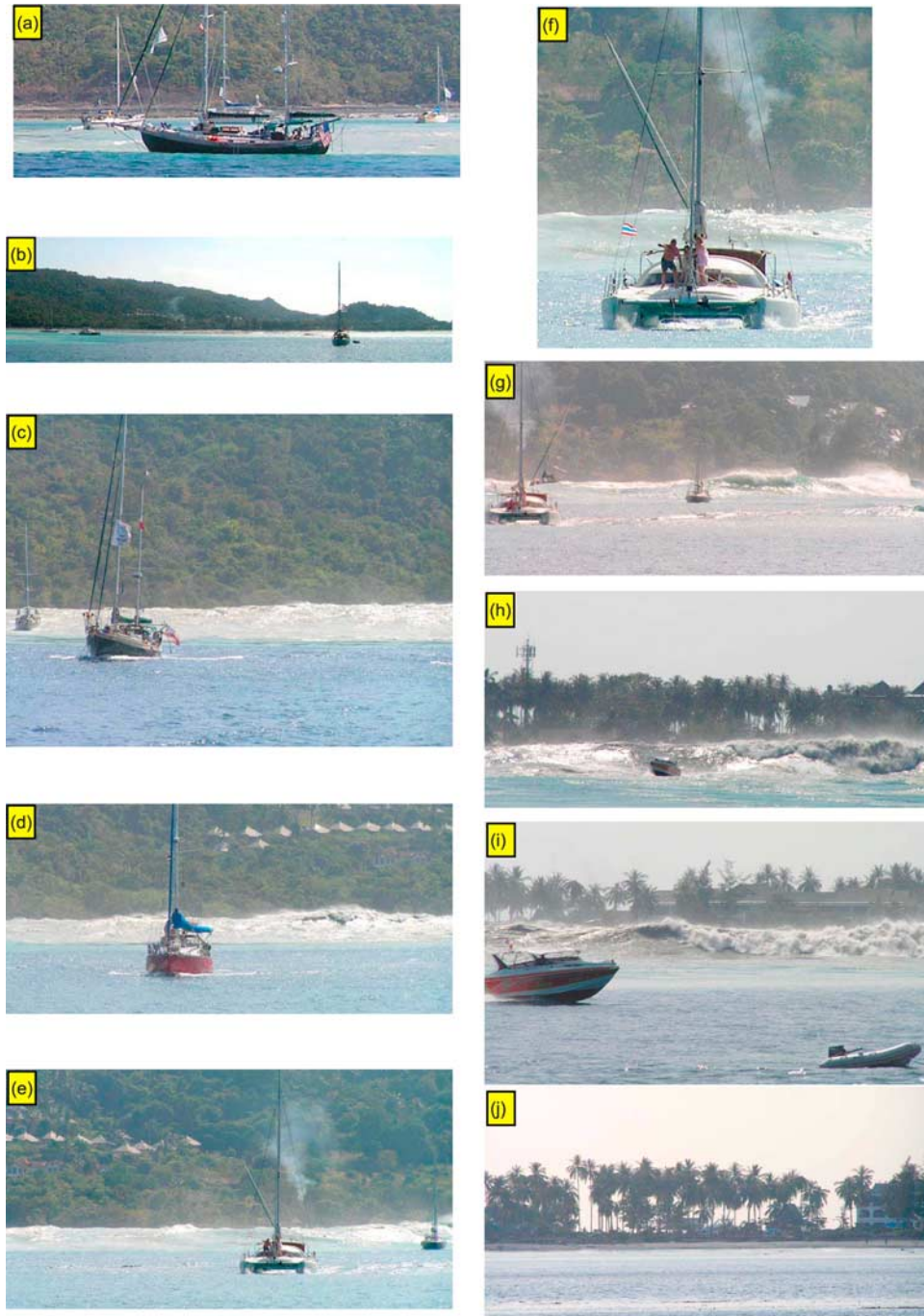
Figure 13. Arrival of 26 December 2004 tsunami on Ko Phi Phi's north shore, starting at approximately 10h45′ local time and covering 5′ from Figure 13a to 13i, seen from yacht *Gaultine III* (black arrow in Figure 7). (a, b) Facing east, the initial depression wave has exposed the reef; (c, d, e) The first elevation wave moves toward southeast and reflects off the eastern cliff and (f) closeup of Figure 13e. (g) Reflected wave moves down the shore and breaks. (h) Breaking edge wave is moving westward down the sand isthmus. (i) Wave attacks resort on west side and (j) the morning after. (Pictures taken by Lou Evans, http://www.yachtaragorn.com/Thailand.htm.)

al., 2001, 2002]. In this section, we utilize this distribution adjusted for runup observations, as a benchmark to examine the degradation of simulated runups with decreasing grid resolution. We examine both the deviation of lower resolution results from the distribution as well as the deviation of

model predictions from the distribution obtained at the highest resolution.

[51] The log-normal distribution for runup elevations r is defined in terms of the mean a and variance σ^2 of N natural logarithm of runup values $\xi_i = \ln r_i$ (for $i = 1, \cdots, N$). The
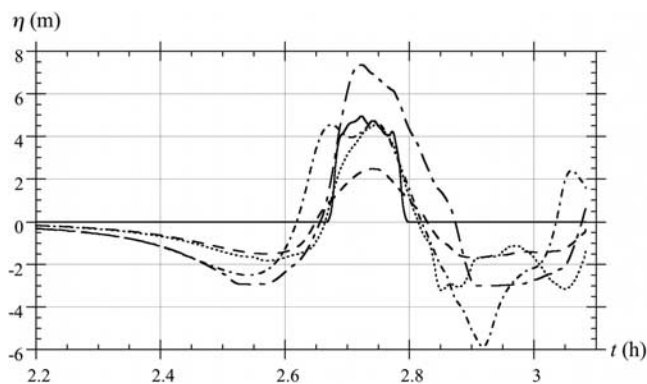
Figure 14. Free surface elevation (in meters) simulated at points located in Figure 7 (bottom right). The northern wave arrives from N1 (short-dash–dotted line, 10 m bathymetry) to N2 (long-dash–dotted line, 3 m) in Lohdalum Bay. In the south, the wave arrives from S1 (dashed line, 16 m bathymetry) to S2 dotted line, 12 m) in the Tonsai Bay. Location L0 (solid line) is originally a land point (2.5 m topography). This point is flooded at 2h40′ during approximately 6.5′. The curve at N2 reaches the local bottom (3 m) at 2h31′ during 5′, and again at 2h54′ for 6′, indicating full reef emergence.

probability density function for the ξ population is then hypothesized to be the normal distribution,

$$p(\xi) = \frac{1}{\sigma\sqrt{2\pi}} \exp\left(\frac{(\xi - a)^2}{2\sigma^2}\right). \qquad (4)$$

Results comparing data to this distribution are usually written in terms of the probability of exceedance, given by

$$F(\xi) = \int_\xi^\infty p(\xi')\,d\xi' = \frac{1}{2}\mathrm{erf}\left(\frac{\xi - a}{\sqrt{2}\sigma}\right). \qquad (5)$$

[52] We performed this analysis for both the data in Table 3 and runup values predicted using the different grid resolutions. Figure 15 shows that, despite the small number of points, both the (58) observed runups in Thailand and those predicted continuously over the geographic regions of Figure 3, using the 0.25′ model grid, follow similar log-normal distributions, whereas runups predicted in the coarser grids do not agree well with the observed distribution, with results degrading monotonically with loss of resolution. *Choi et al.* [2001, 2002] commented that the fact observed runups followed well the log-normal distribution indicated that they were governed by "random coastal bathymetry and coastline." In our model, the fact that runup predictions in the 0.25′ grid also follow this distribution indicates that the natural variability of the governing parameters (i.e., bathymetry and coastline geometry) is well represented in this grid, whereas it is underresolved in the coarser grids, leading to systematic bias in the simulations.

6.2. Dispersion

[53] *Grilli et al.* [2007] studied effects of frequency dispersion in their 1′ ocean-wide grid, by comparing FUN-WAVE to nondispersive Nonlinear Shallow Water Equations (NSWE; Appendix A) results. They found weak but significant dispersive effects on crest geometry and height distribution of westward propagating tsunami waves. To estimate dispersive effects in our 0.25′ grid, we similarly performed tsunami simulations using a NSWE model. Runups thus computed are shown as symbols on Figures 2–4 and, in view of the small differences with earlier results of the Boussinesq model, we conclude that dispersive effects are not a dominant process in coastal Thailand. Figure 16 further shows that up to 25% dispersive effects may occur, but only very locally, which may be associated with local topographic features, but these do not significantly affect maximum runup values, although the timing and wave sequences could still be significantly affected by dispersion.

7. Conclusions

[54] We used a coseismic tsunami source, which was developed and validated earlier by *Grilli et al.* [2007] on a 1′ ocean-basin-scale grid, to perform higher resolution regional simulations of tsunami impact in coastal Thailand, for the tsunami generated during the 12/26/04 event. *Grilli et al.* [2007] calibrated this tsunami source to best fit: (1) time series of surface elevation measured at a number of tide gauges and (2) surface elevation measured along one satellite transect in the Indian Ocean. Since runup observations were not used in the calibration, the present simulations provide the runup distribution in coastal Thailand in a predictive mode. We found that, at the finer selected grid scale (0.25′), simulated runups are in very good agreement with (58) runups measured during post-tsunami field surveys, and nearly reproduce their expected log-normal statistical distribution. Simulations performed in a series of coarser
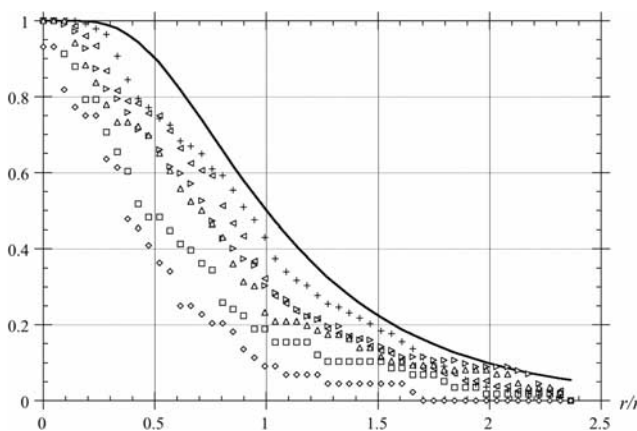

Figure 15. Cumulative probability of simulated runup r normalized by $r^* = \exp(\overline{\ln r}) = 5.41$ m compared to the theoretical log-normal distribution for observed data in Table 2. Solid line is distribution based on observed data. Grid resolutions: plus, 0.25′; left-pointing triangle, 0.5′; right-pointing triangle, 0.75′; up-pointing triangle, 1.0′; square, 1.5′; diamond, 2.0′.
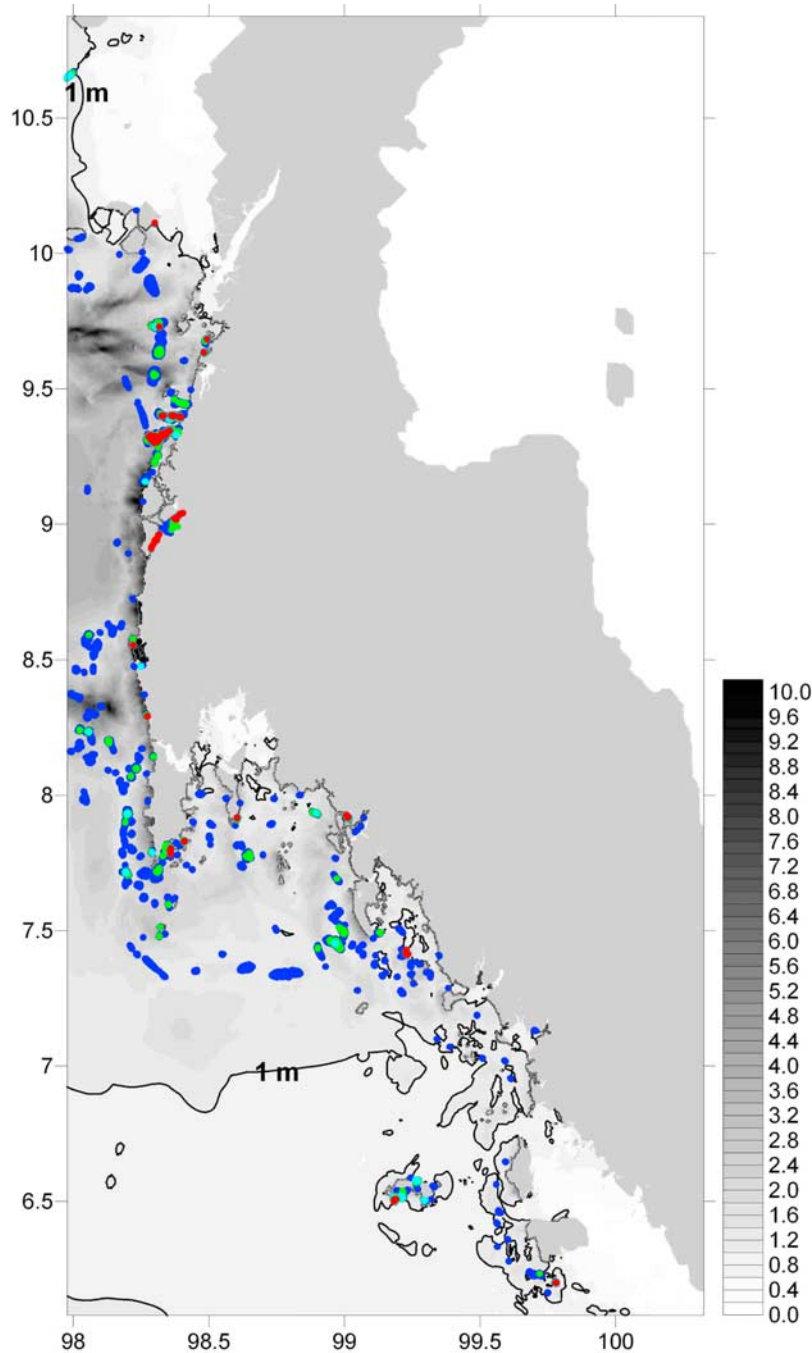
Figure 16. Maximum surface elevations (in meters) computed during the 5-hour simulation in the 0.25′ grid, with the Boussinesq model (background), as compared to the Nonlinear Shallow Water solution. A threshold of 1 m of maximum elevation above which the comparison is applied, delimited by light dark lines. The relative difference between these solutions is marked as contour lines of percentages, although these appear as dots or patches on the figure, because they are very localized in space. The most frequent differences, 10−15%, are marked in blue, green is used for 15−20%, cyan blue for 20−25% and red for ≥25% differences.

model grids exhibited a gradual deterioration of the model predictive ability, and hence confirmed the relevance of the selected 0.25′ grid scale. A more detailed case study was performed for Ko Phi Phi, an island of particularly complex geometry, where eyewitnesses reported a complex tsunami arrival, for which two picture sequences as well as a few measured runups were available. We found that the model was able to account for all these diverse observations and provide a clear picture of what happened in Phi Phi island on that fateful day.

[55] Despite using a dispersive wave model (FUNWAVE), frequency dispersion does not appear to significantly affect

Figure 17. SPOT-5 satellite picture of Suk Samran on 24 December 2005 (Figure 2). (Courtesy of Centre National d'Etudes Spatiales, France).

runups in Thailand, although timing and sequences of waves could be more significantly affected. Therefore the success of the present simulations mostly results from the proper calibration of the tsunami source, the accurate bathymetric data used in coastal Thailand, and the parameterization of FUNWAVE's coastal wave transformation algorithms to accurately simulate tsunami runup and inundation (performed as part of earlier regional tsunami case studies).

[56] In view of the simulation robustness and accuracy, we posit that results shown in Figures 3 and 7 provide a synoptic picture of tsunami impact, as it occurred in Thailand during the 12/26/04 event, which can reasonably be used in lieu of field data in locations where post-tsunami surveys have not been conducted. Hence these results could be used to identify areas of significant tsunami impact, where further field surveys should be conducted. Most of the observations so far in Thailand have indeed been made in locations where heavy casualties were reported, such as Khao Lak, Patong Beach, and Phi Phi island, which are also areas with important tourist related infrastructures. There were very few observations made outside these areas. Our results (Figure 3), for instance, predict large runups in excess of 10 m at a few locations north of Ban Na Thai and south of Khao Lak (8.2°–8.6°N). However, there are no observations or even eyewitness reports to compare with in those locations, except in Khao Lak-Lamru, where it was reported that a tide gauge was destroyed. Similarly, further north at ~9.1°N, our model predicts 13–20 m runups along the west coast of the island of Ko Pra Thong (Figure 2). Although no data have been published yet for this area,

some recent field surveys still being processed, report very large runups of this order of magnitude in this area of Ko Pra Thong [Beitel and Moran, personal communication]. A last example is Figure 17, which shows a satellite picture of the Suk Samran area, at ~9.5°N, taken one year after the tsunami hit: although no runup measurements were made, the picture still shows that severe damage occurred west of this location, where our model predicts a localized 5 m runup.

[57] Besides pointing at large potential runups, model results also identify less vulnerable or sheltered regions, for example, south and east of Phuket Island. In that area, the model predicts moderate runups, ranging from 1 to 2 m, which could represent important information for coastal redevelopment plans. Such redevelopment activities, however, would have to be more carefully planned, for instance on the basis of simulated tsunami hazard maps developed using even finer grids in complex topographic settings.

[58] The probability of recurrence of such a catastrophic tsunami event is not known. However, in view of the tectonics of the region, one can safely assume that an event similar to the 12/26/04 tsunami will happen some time in the future. At present, regions of Thailand vulnerable to tsunami impact have been identified as those regions that suffered heavy casualties or where large runups were measured. On the basis of our results, however, we posit that other regions that were not surveyed and are not yet developed or properly covered by a land-use plan, may be similarly vulnerable. It is a worldwide trend that more and more urban areas are developed along coastlines, and is thus of prime importance to identify all vulnerable coastal areas in Thailand, that may be considered for development in the future.

Appendix A: Boussinesq Model Equations in FUNWAVE

[59] The Boussinesq model equations implemented in FUNWAVE are based on the work of *Wei et al.* [1995], with extensions to cover bottom friction, breaking and shoreline runup effects developed by *Chen et al.* [2000] and *Kennedy et al.* [2000]. The equation for volume conservation is given by

$$\beta\eta_t + \nabla_h \cdot \mathbf{M} = 0, \tag{A1}$$

where $\eta(x, y, t)$ represents surface displacement away from local mean depth $h(x, y)$, ∇_h represents a gradient in horizontal coordinates (x, y), and $\mathbf{M}$ represents depth-integrated horizontal volume flux. $\mathbf{M}$ is given by

$$\mathbf{M}/\Lambda = \mathbf{u}_\alpha + \left(\frac{z_\alpha^2}{2} - \frac{1}{6}\left(h^2 - h\eta + \eta^2\right)\right)\nabla_h A$$
$$+ \left(z_\alpha + \frac{1}{2}(h - \eta)\right)\nabla_h B. \tag{A2}$$

Here $\mathbf{u}_\alpha$ denotes the horizontal velocity at an elevation z_α defined with z oriented upward from the free surface, here

taken to be $z_\alpha = -0.531h$, following *Wei et al.* [1995]. A and B are functions of velocity given by

$$A = \nabla_h \cdot \mathbf{u}_\alpha \tag{A3}$$

$$B = \nabla_h \cdot (h\mathbf{u}_\alpha). \tag{A4}$$

The factors β and Λ were introduced by *Kennedy et al.* [2000] and *Chen et al.* [2000] to implement a porous (i.e., absorbing) beach method, used to keep the subaerial portion of the model grid computationally active and to simplify the calculation of runup on dry shorelines. These are given by

$$\beta = \begin{cases} 1, & \eta \geq z^* \\ \delta + (1-\delta)e^{\lambda(\eta-z^*)/h_0}, & \eta < z^* \end{cases} \tag{A5}$$

and $\Lambda =$

$$\begin{cases} (\eta - z^*) + \delta(z^* + h_0) + \dfrac{(1-\delta)h_0}{\lambda}\left(1 - e^{-\lambda\left(1 + z^*/h_0\right)}\right); & \eta \geq z^* \\ \delta(\eta + h_0) + \dfrac{(1-\delta)h_0}{\lambda}e^{\lambda(\eta-z^*)/h_0}\left(1 - e^{-\lambda(1+\eta/h_0)}\right); & \eta < z^*. \end{cases} \tag{A6}$$

Here h_0 represents the depth down to which the porosity of the beach extends, which must be deeper than the depth of maximum wave rundown during a calculation. The choice of z^* is discussed by *Kennedy et al.* [2000]. Here $\delta = 0.08$ and $\lambda = 25$, based on studies of a number of tsunami runup events [*Watts et al.*, 2003; *Day et al.*, 2005].

[60] The momentum equations are given by

$$\mathbf{u}_{\alpha t} + (\mathbf{u}_\alpha \cdot \nabla_h)\mathbf{u}_\alpha + g\nabla_h\eta + \mathbf{V}_1 + \mathbf{V}_2 + \mathbf{R}_f - \mathbf{R}_b = 0, \tag{A7}$$

where $\mathbf{V}_1$ and $\mathbf{V}_2$ represent dispersive effects and are given by

$$\mathbf{V}_1 = \frac{z_\alpha^2}{2}\nabla_h A_t + z_\alpha \nabla_h B_t - \nabla_h\left[\frac{\eta^2}{2}A_t + \eta B_t\right] \tag{A8}$$

$$\mathbf{V}_2 = \nabla_h\left[(z_\alpha - \eta)(u_\alpha \cdot \nabla_h)B + \frac{1}{2}(z_\alpha^2 - \eta^2)(u_\alpha \cdot \nabla_h)A\right] + \frac{1}{2}\nabla_h\left[(B + \eta A)^2\right], \tag{A9}$$

where $\mathbf{R}_b$ and $\mathbf{R}_f$ represent forces arising from wave breaking and bottom friction, respectively, and are explained by *Kennedy et al.* [2000].

[61] Nonlinear shallow water (NSW) equations follow from the above by neglecting terms representing frequency dispersion, leading to the results

$$\mathbf{M} = \Lambda\mathbf{u}_\alpha \tag{A10}$$

$$\mathbf{V}_1 = \mathbf{V}_2 = 0. \tag{A11}$$

This formulation is included as a regular option in the FUNWAVE code.

[62] FUNWAVE as used here does not include a moving bottom, and tsunami signals are introduced as static surface elevation displacements. In the event of multiple sources with staggered initial times, each source is introduced by linearly superimposing it on the already evolving wave field. This effectively eliminates any nonlinear effects arising during the initial upthrust of the water column above each source.

[63] The version of FUNWAVE used here does not utilize the revision of dispersive terms discussed by *Chen et al.* [2003], which incorporates an improved representation of vorticity. The problem studied here, with propagation based on an initial static source, is essentially irrotational, and differences between the models would not be apparent until after interaction between the tsunami wave front and inundated shorelines.

References

Ammon, C. J., et al. (2005), Rupture process of the 2004 Sumatra-Andaman earthquake, *Science*, *308*, 1133–1139.

Bagai, D. S., et al. (2005), Tsunami Thailand one year after international response and contribution of international partners, report, 120 pp., U. N. Dev. Programme, New York. (Available at http://www.undp.or.th/publications/index.html)

Bilham, R. (2005), A flying start, then a slow slip, *Science*, *308*, 1126–1127.

Bilham, R., E. R. Engdahl, N. Feldl, and S. P. Satyabala (2005), Partial and complete rupture of the Indo-Andaman plate boundary 1847–2004, *Seismol. Res. Lett.*, *76*, 29,911–29,932.

Chen, Q., J. T. Kirby, R. A. Dalrymple, A. B. Kennedy, and A. Chawla (2000), Boussinesq modeling of wave transformation, breaking, and run-up. II: 2D, *J. Waterw. Port Coastal Ocean Eng.*, *126*(1), 48–56.

Chen, Q., J. T. Kirby, R. A. Dalrymple, F. Shi, and E. B. Thornton (2003), Boussinesq modeling of longshore currents, *J. Geophys. Res.*, *108*(C11), 3362, doi:10.1029/2002JC001308.

Choi, B. H., S. J. Hong, and E. Pelinovsky (2001), Simulation of prognostic tsunamis on the Korean coast, *Geophys. Res. Lett.*, *28*, 2013–2016.

Choi, B. H., E. Pelinovsky, I. Ryabov, and S. J. Hong (2002), Distribution functions of tsunami wave heights, *Nat. Hazards*, *25*, 1–21.

Choi, B. H., J. H. Sung, and E. Pelinovsky (2006), Distribution of runup heights of the December 26, 2004 tsunami in the Indian Ocean, *Geophys. Res. Lett.*, *33*, L13601, doi:10.1029/2006GL025867.

Day, S. J., P. Watts, S. T. Grilli, and J. T. Kirby (2005), Mechanical models of the 1975 Kalapana, Hawaii earthquake and tsunami, *Mar. Geol.*, *215*(1)–(2), 59–92.

ETOPO2 (2001), ETOP02: 2-minute gridded global relief data (2001), http://www.ngdc.noaa.gov/mgg/fliers/01mgg04.html, World Data Cent. for Mar. Geol. and Geophys., Boulder, Colo.

Fujii, Y., and K. Satake (2007), Tsunami source of the 2004 Sumatra-Andaman earthquake inferred from tide gauge and satellite data, *Bull. Seismol. Soc. Am.*, *97*(1a), 192–207, doi:10.1785/0120050613.

Garay, M. J., and D. J. Diner (2007), Analysis of multi-angle imaging spectroradiometer (MISR) time-lapse imagery of tsunami waves from the 26 December 2004 Sumatra-Andaman earthquake, *Remote Sens. Environ.*, *107*(1–2), 256–263, doi:10.1016/j.rse.2006.10.022.

Gower, J. (2005), Jason 1 detects the 26 December 2004 tsunami, *Eos Trans. AGU*, *86*(4), 37.

Grilli, S. T., M. Ioualalen, J. Asavanant, F. Shi, J. T. Kirby, and P. Watts (2007), Source constraints and model simulation of the December 26, 2004 Indian Ocean tsunami, *J. Waterw. Port Coastal Ocean Eng.*, in press.

Hirata, K., K. Satake, Y. Tanioka, K. Tsurane, Y. Hasegawa, Y. Hayashi, and N. Hamada (2006), The 2004 Indian Ocean tsunami: Tsunami source model from satellite altimetry, *Earth Planets Space*, *58*(2), 195–201.

Ioualalen, M., B. Pelletier, M. Regnier, and P. Watts (2006), Numerical modeling of the 26th November 1999 Vanuatu tsunami, *J. Geophys. Res.*, *111*, C06030, doi:10.1029/2005JC003249.

Kennedy, A. B., Q. Chen, J. T. Kirby, and R. A. Dalrymple (2000), Boussinesq modeling of wave transformation, breaking, and run-up. I: 1D, *J. Waterw. Port Coastal Oceanic Eng.*, *126*(1), 39–47.

Kirby, J. T. (2003), Boussinesq models and applications to nearshore wave propagation, surf zone processes and wave-induced currents, in *Advances in Coastal Modeling*, *Oceanogr. Ser.*, vol. 67, edited by V. C. Lakhan, pp. 1–41, Elsevier, New York.

Lay, T., et al. (2005), The great Sumatra-Andaman earthquake of 26 December 2004, *Science*, *308*, 1127–1132.

Merrifield, M. A., et al. (2005), Tide gauges observations of the Indian Ocean tsunami, December 26, 2004, *Geophys. Res. Lett.*, *32*, L09603, doi:10.1029/2005GL022610.

Nagarajan, B., I. Suresh, D. Sundar, R. Sharma, A. K. Lal, S. Neetu, S. S. C. Shenoi, S. R. Shetye, and D. Shankar (2006), The great tsunami of 26 December 2004: A description based on tide-gauge data from the Indian subcontinent and surrounding areas, *Earth Planets Space*, *58*(2), 211–215.

Okada, S. (1985), Surface displacement due to shear and tensile faults in a half-space, *Bull. Seismol. Soc. Am.*, *75*, 1135–1154.

Papadopoulos, G. A., et al. (2006), The large tsunami of 26 December 2004: Field observations and eyewitness accounts from Sri Lanka, Maldives Is. and Thailand, *Earth Planets Space*, *58*, 233–241.

Smith, W. H. F., R. Scharroo, V. V. Titov, D. Arcas, and B. K. Arbic (2005), Satellite altimeters measure tsunami: Early model estimates confirmed, *Oceanography*, *18*(2), 11–13.

Socquet, A., C. Vigny, N. Chamot-Rooke, W. Simons, C. Rangin, and B. Ambrosius (2006), India and Sunda plates motion and deformation along their boundary in Myanmar determined by GPS, *J. Geophys. Res.*, *111*, B05406, doi:10.1029/2005JB003877.

Stein, S., and E. Okal (2005), Speed and size of the Sumatra earthquake, *Nature*, *434*, 581–582.

Tsuji, Y., Y. Namegaya, H. Matsumoto, S. Iwasaki, W. Kanbua, M. Sriwichai, and V. Meesuk (2006), The 2004 Indian tsunami in Thailand: Surveyed runup heights and tide gauges records, *Earth Planets Space*, *58*(2), 223–232.

Van Dorn, W. G. (1965), Tsunamis, *Adv. Hydrosci*, *2*, 1–48.

Vigny, C., et al. (2005), Insight into the 2004 Sumatra-Andaman earthquake from GPS measurements in southeast Asia, *Nature*, *436*, 201–206.

Watts, P., S. T. Grilli, J. T. Kirby, G. J. Fryer, and D. R. Tappin (2003), Landslide tsunami case studies using a Boussinesq model and a fully nonlinear tsunami generation model, *Nat. Hazards Earth Syst. Sci.*, *3*(5), 391–402.

Waythomas, C. F., and P. Watts (2003), Simulation of tsunami generation by pyroclastic flow at Aniakchak Volcano, Alaska, *Geophys. Res. Lett.*, *30*(14), 1751, doi:10.1029/2003GL017220.

Wei, G., and J. T. Kirby (1995), A time-dependent numerical code for extended Boussinesq equations, *J. Waterw. Port Coastal Oceanic Eng.*, *121*, 251–261.

Wei, G., J. T. Kirby, S. T. Grilli, and R. Subramanya (1995), A fully nonlinear Boussinesq model for free surface waves. Part 1: Highly nonlinear unsteady waves, *J. Fluid Mech.*, *294*, 71–92.

————————

J. Asavanant and N. Kaewbanjak, Department of Mathematics, Chulalongkorn University, Bangkok 10330, Thailand. (ajack@chula.ac.th)

S. T. Grilli, Department of Ocean Engineering, University of Rhode Island, Narragansett, RI 02882, USA. (grilli@oce.uri.edu)

M. Ioualalen, Geosciences Azur, 2 quai de la Darse, BP. 48, F-06230 Villefranche-sur-mer, France. (mansour.ioualalen@geoazur.obs-vlfr.fr)

J. T. Kirby, Center for Applied Coastal Research, University of Delaware, Newark, DE 19716, USA. (kirby@udel.edu)

P. Watts, Applied Fluids Engineering, Inc., 5710 East 7th Street, Long Beach, CA 90803, USA. (phil.watts@appliedfluids.com)